nature immunology

Article

https://doi.org/10.1038/s41590-023-01543-9

Neoantigen-specific stem cell memory-like CD4$^+$ T cells mediate CD8$^+$ T cell-dependent immunotherapy of MHC class II-negative solid tumors

Received: 8 March 2023

Accepted: 22 May 2023

Published online: 3 July 2023

Check for updates

A list of authors and their affiliations appears at the end of the paper

CD4$^+$ T cells play key roles in a range of immune responses, either as direct effectors or through accessory cells, including CD8$^+$ T lymphocytes. In cancer, neoantigen (NeoAg)-specific CD8$^+$ T cells capable of direct tumor recognition have been extensively studied, whereas the role of NeoAg-specific CD4$^+$ T cells is less well understood. We have characterized the murine CD4$^+$ T cell response against a validated NeoAg (CLTC$_{H129>Q}$) expressed by the MHC-II-deficient squamous cell carcinoma tumor model (SCC VII) at the level of single T cell receptor (TCR) clonotypes and in the setting of adoptive immunotherapy. We find that the natural CLTC$_{H129>Q}$-specific repertoire is diverse and contains TCRs with distinct avidities as measured by tetramer-binding assays and CD4 dependence. Despite these differences, CD4$^+$ T cells expressing high or moderate avidity TCRs undergo comparable in vivo proliferation to cross-presented antigen from growing tumors and drive similar levels of therapeutic immunity that is dependent on CD8$^+$ T cells and CD40L signaling. Adoptive cellular therapy (ACT) with NeoAg-specific CD4$^+$ T cells is most effective when TCR-engineered cells are differentiated ex vivo with IL-7 and IL-15 rather than IL-2 and this was associated with both increased expansion as well as the acquisition and stable maintenance of a T stem cell memory (T$_{SCM}$)-like phenotype in tumor-draining lymph nodes (tdLNs). ACT with T$_{SCM}$-like CD4$^+$ T cells results in lower PD-1 expression by CD8$^+$ T cells in the tumor microenvironment and an increased frequency of PD-1$^+$CD8$^+$ T cells in tdLNs. These findings illuminate the role of NeoAg-specific CD4$^+$ T cells in mediating antitumor immunity via providing help to CD8$^+$ T cells and highlight their therapeutic potential in ACT.

Neoantigen (NeoAg)-specific T cells are frequently observed in the tumor microenvironment (TME) and periphery of human patients with cancer before and during treatment with immunotherapies such as immune checkpoint blockade (ICB) and personalized cancer vaccines[1–8]. While it is known that NeoAg-specific CD8$^+$ T cells are capable of directly recognizing and destroying tumor cells, clinical responses have also been observed in patients receiving adoptive cellular therapy (ACT) with autologous tumor-infiltrating lymphocytes

e-mail: sps@lji.org

https://doi.org/10.1038/s41590-023-01543-9

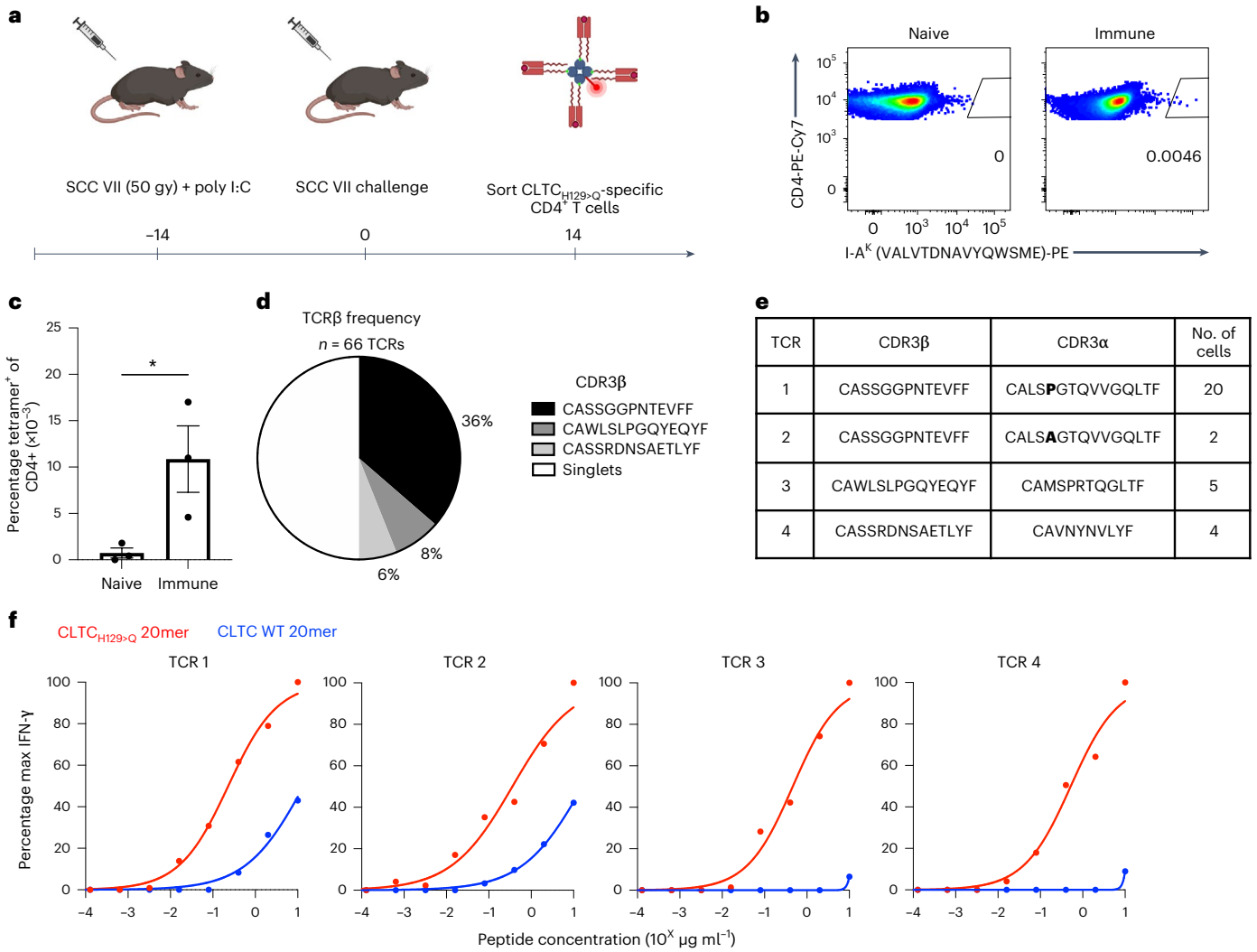

TCR	CDR3β	CDR3α	No. of cells
1	CASSGGPNTEVFF	CALS**P**GTQVVGQLTF	20
2	CASSGGPNTEVFF	CALS**A**GTQVVGQLTF	2
3	CAWLSLPGQYEQYF	CAMSPRTQGLTF	5
4	CASSRDNSAETLYF	CAVNYNVLYF	4

Fig. 1 | Identification and validation of CLTC$_{H129>Q}$-specific CD4$^+$ T cell clones from SCC VII. a, Schematic overview of tetramer sorting experiments to isolate CLTC$_{H129>Q}$-specific T cells. **b**, Representative flow cytometry plots of tetramer-binding CD4$^+$ T cells from naive or SCC VII-immune mice. **c**, Quantification of tetramer-positive CD4$^+$ T cells from the spleens of naive or immunized mice; mean ± s.e.m. of three individual mice; *P = 0.049 two-tailed unpaired t-test. **d**, TCR β-chain diversity of tetramer-sorted T cells. **e**, CDR3 sequences for α- and β-chains of clonally expanded T cells. **f**, Concentration–response curves of IFN-γ production by primary CD4$^+$ T cells retrovirally transduced with each CLTC$_{H129>Q}$-specific TCR stimulated with splenocytes pulsed with either mutant or wild-type peptides. Data are representative of three independent experiments.

(TILs) containing NeoAg-specific CD4$^+$ T cells, suggesting that CD4$^+$ T cells also play a crucial role in directing tumor immune responses[9–11]. In human melanoma, infiltration of NeoAg-specific CD4$^+$ T cells is associated with antitumor effector phenotypes of macrophages, B cells and CD8$^+$ T cells[12]. Several mechanisms of antitumor immunity mediated by CD4$^+$ T cells have been proposed by studies in mouse models, including direct cytotoxicity dependent on recognition of MHC-II$^+$ tumor cells, local secretion of effector cytokines in the TME and providing T cell help for CD8$^+$ T cells[13–15]; however, how key characteristics such as TCR avidity and cellular differentiation states impact CD4$^+$ T cell-mediated antitumor immunity remains unknown.

In the present study, we identified four distinct TCR clonotypes recognizing an epitope derived from a mutated clathrin heavy chain gene (CLTC$_{H129>Q}$) in the SCC VII tumor model. We found that CLTC$_{H129>Q}$-specific T cell receptors (TCRs) differed in their avidity for antigen but were nonetheless similarly able to undergo antigen-dependent expansion in vivo and provide CD8$^+$ T cell- and CD40L-dependent protection from tumor challenge. Furthermore, treatment with interleukin (IL)-7 and IL-15 induced a durable T stem cell memory (T_{SCM})-like phenotype in TCR-engineered CLTC$_{H129>Q}$-specific CD4$^+$ T cells, enabling these cells to effectively control tumors in the therapeutic setting, highlighting the clinical relevance of TCR-engineered CD4$^+$ T cells recognizing tumor-derived NeoAg.

Results

Expansion of CLTC$_{H129>Q}$-specific CD4$^+$ T cells correlates with protective whole-cell vaccination

We have previously demonstrated that vaccination with irradiated SCC VII cells and adjuvant polyI:C is protective against subsequent live tumor challenge. SCC VII-immune mice generate CD4$^+$ and CD8$^+$ NeoAg-specific T cell responses, which includes recognition of a mutated clathrin heavy chain epitope (CLTC$_{H129>Q}$) by CD4$^+$ T cells[16]. To identify TCRs from CLTC$_{H129>Q}$-specific CD4$^+$ T cells, C3H/HeJ mice were immunized with irradiated SCC VII tumor cells admixed with polyI:C and challenged 14 d later with live SCC VII cells. At 14 d after tumor challenge, splenocytes from immune mice were isolated and stained with a CLTC$_{H129>Q}$/I-A^K tetramer (Fig. 1a and Extended Data Fig. 1a). Consistent with our previous ELISpot results, tetramer-positive CD4$^+$

T cells were present at a significantly increased frequency in SCC VII-immune mice compared to naive mice (Fig. 1b,c).

Identification of $CLTC_{H129>Q}$-specific $CD4^+$ T cell clonotypes

To isolate $CLTC_{H129>Q}$-specific $CD4^+$ T cells, single tetramer-positive cells from challenged and protected mice were sorted into 96-well plates and the CDR3 regions of both TCR α/β-chains were amplified by PCR as previously described[17]. Sequencing of complementary DNA libraries revealed three expanded TCR β clonotypes represented among tetramer-sorted cells (Fig. 1d). These three TCR β-chains paired with four distinct α-chains, corresponding to four unique expanded T cell clones (Fig. 1e). Of note, TCR 1 and TCR 2 shared the same TCR β-chain and nearly identical α-chains, which differ at a single alanine to proline substitution within the CDR region. To confirm TCR surface assembly and specificity, each α/β receptor was expressed via retroviral transduction of naive primary C3H $CD4^+$ T cells and tested for recognition of wild-type versus H129 > Q forms of the $CLTC_{119–133}$ peptide. $CD4^+$ T cells expressing each of the four TCRs produced interferon (IFN)-γ when stimulated with splenocytes pulsed with the H129 > Q peptide (Fig. 1f) but produced less or no detectable IFN-γ in response to the wild-type epitope.

$CLTC_{H129>Q}$-specific TCRs differ in avidity

Next, we set out to compare the functional characteristics of the $CLTC_{H129>Q}$-specific TCRs. For all four populations of transduced primary $CD4^+$ T cells, >79% of cells expressed the introduced TCR as evidenced by staining for the associated TCR β-chain variable regions (TRBVs) (Fig. 2a). Gating on the TRBV-expressing cells revealed a consistent difference in tetramer binding, with both a greater frequency and magnitude of tetramer binding observed for cells expressing TCRs 1 and 2 than those expressing TCRs 3 and 4 (Fig. 2a). Indeed, the median fluorescence intensity (MFI) of tetramer binding for cells expressing TCR 1 was significantly greater than that of cells expressing either TCR 3 or TCR 4 (22.8× and 12.1× greater, respectively) (Fig. 2b and Extended Data Fig. 1b). To further investigate the avidity differences between TCRs, we incubated transduced primary T cells with a titration of tetramer concentrations and measured the percent of maximal fluorescence at each concentration (Fig. 2c). These experiments were consistent with our initial observations, indicating that both TCRs 1 and 2 had significantly lower tetramer half-maximum effective concentration (EC_{50}) values than TCRs 3 and 4 (Fig. 2d). To study the TCR-binding properties in the absence of CD4, we transduced the TCR-deficient $CD8^+$ T cell hybridoma line 58α$^-$β$^-$ with each TCR. The 58α$^-$β$^-$ cells expressing TCRs 1 and 2 were able to bind tetramer independently of the CD4 co-receptor, whereas cells expressing TCRs 3 and 4 did not, despite comparable levels of TCR expression (Fig. 2e). In conclusion, the $CLTC_{H129>Q}$-specific $CD4^+$ T cell pool contains T cell clones expressing both high and moderate avidity antigen receptors.

Differences in TCR avidity do not correlate with differences in proximal TCR signaling in vitro

Given the differences in TCR avidity observed, we investigated whether these correlate with proximal TCR signaling, as has been demonstrated in studies of tumor-specific $CD8^+$ T cells[18]. To measure levels of TCR signaling, we stained permeabilized TCR-expressing primary $CD4^+$ T cells for phosphorylated ERK1/2 (pERK1/2) after a brief stimulation period with peptide-pulsed splenocytes. While all four groups of TCR-expressing $CD4^+$ T cells expressed higher levels of pERK1/2 after stimulation with peptide-pulsed splenocytes compared to splenocytes without added peptide, there were no significant differences in the percentage of activated cells between different TCRs (Fig. 2f). These results suggest that differences in $CLTC_{H129>Q}$-specific TCR avidity do not correlate with differences in proximal TCR signaling.

Expansion and activation of $CLTC_{H129>Q}$-specific $CD4^+$ T cells in vivo is TCR avidity independent

To investigate how differences in TCR avidity may impact antigen-specific responses in vivo, we transferred equal numbers of CellTrace Violet (CTV)-labeled $CD4^+$ T cells expressing either TCR 1 or TCR 3 into either naive mice or mice that were subsequently challenged with SCC VII. In this experimental system we were able to differentiate between cells expressing TCR 1 or TCR 3 as either $CD90.1^+TRBV8.3^+$ or $CD90.1^+TRBV8.3^-$, respectively (Fig. 3a,b). Antigen-specific expansion of adoptively transferred cells was apparent within 3 d, as the frequency of total $CD90.1^+$ cells in tumor-draining lymph nodes (tdLNs) increased significantly in mice challenged with live SCC VII cells compared to naive animals (Fig. 3c). We found that cells expressing TCR 1 or TCR 3 proliferated to a similar extent in the context of antigen derived from live tumor cells, with no significant differences in the number of expanded CTV^{low} cells in mice challenged with SCC VII (Fig. 3d). Neither $CD4^+$ T cell population proliferated significantly in naive mice, suggesting that TCR 1 does not recognize the wild-type CLTC epitope in vivo despite producing IFN-γ in response to splenocytes pulsed with high concentrations of the corresponding peptide (Figs. 3d and 1f). Consistent with these results, the relative frequency of cells expressing either TCR 1 or TCR 3 did not change significantly in either naive mice or mice challenged with SCC VII compared to their starting frequencies (Fig. 3e). In addition, both TCR1- and TCR 3-expressing cells upregulated similar levels of the acute activation marker CD69 in an antigen-specific manner (Extended Data Fig. 2a,b). Altogether, these results suggest that NeoAg-specific $CD4^+$ T cells with distinct TCRs behave similarly in vivo independent of TCR avidity.

Next, we investigated the impact of TCR avidity on T cell activation in the TME. tdLNs and tumors were collected from mice 10 d after SCC VII challenge to assess the relative frequency and activation phenotype of cells expressing either TCR 1 or TCR 3 (Fig. 3f). Consistent with our results with cells collected after 3 d, there was no significant difference in the relative frequencies of cells expressing each TCR in the tdLN or TME after 10 d (Fig. 3g). Expression of co-inhibitory markers such as PD-1 is a hallmark of both tumor-reactive $CD4^+$ and $CD8^+$ T cells in the TME. We determined that cells expressing either TCR 1 or TCR 3 expressed similar levels of PD-1 in the TME and both expressed significantly more PD-1 than $CD90.1^-$ host $CD4^+$ T cells (Fig. 3h and Extended Data Fig. 2c). These results suggest that the observed differences in TCR avidity do not influence $CD4^+$ T cell persistence or activation in the TME. Given that PD-1 upregulation occurs downstream of TCR signaling, these results also suggest that $CLTC_{H129>Q}$-specific $CD4^+$ T cells are recognizing antigen in the TME as well as the tdLNs.

Fig. 2 | $CLTC_{H129>Q}$-specific TCR avidity, co-receptor dependence and proximal signaling. a, Flow cytometry plots demonstrating expression of the introduced TCRs compared to mock transduced control T cells (top) and tetramer binding (bottom). **b**, MFI of 1 μg ml^{-1} tetramer binding to primary T cells expressing the indicated TCRs. Data represent four independent experiments, $^{**}P = 0.0024$ TCR 1 versus TCR 3, $P = 0.0033$ TCR 1 versus TCR 4 one-way analysis of variance (ANOVA) with Tukey correction for multiple comparisons. NS, not significant. **c**, Tetramer titration plot demonstrating percentage of tetramer-binding cells at indicated tetramer concentrations. Data are representative of four independent experiments. **d**, EC_{50} values determined from tetramer titration curves in **c**. Data represent four independent experiments, $^{**}P = 0.0070$ TCR 1 versus TCR 3, 0.0034 TCR 1 versus TCR 4 one-way ANOVA with Tukey correction for multiple comparisons. **e**, Flow cytometry plots demonstrating TCR expression and tetramer binding of $CD8^+CD4^-$58α$^-$β$^-$ cells expressing each TCR. Data are representative of three independent experiments. **f**, Representative flow cytometry plots of pERK1/2 staining of T cells expressing TCR 1 stimulated with naive splenocytes pulsed with dimethylsulfoxide (DMSO) or 1 μg ml^{-1} $CLTC_{H129>Q}$ peptide (left). Quantification of pERK1/2 staining for each TCR 5 min after stimulation with naive splenocytes pulsed with DMSO or 1 μg ml^{-1} $CLTC_{H129>Q}$ peptide. Data represent three independent experiments. All data represent mean ± s.e.m.

https://doi.org/10.1038/s41590-023-01543-9

$CLTC_{H129>Q}$-specific $CD4^+$ T cell protect from live tumor challenge in a CD40L and $CD8^+$ T cell-dependent manner

We sought to determine whether activated $CLTC_{H129>Q}$-specific $CD4^+$ T cells could protect from live tumor challenge. Notably, SCC VII tumor cells do not express MHC-II and in vitro treatment with IFN-γ did not induce MHC-II expression, suggesting that $CLTC_{H129>Q}$-specific $CD4^+$ T cells are unable to directly recognize tumor cells even under inflammatory conditions in vivo (Fig. 4a). Notably, transfer of 3×10^6

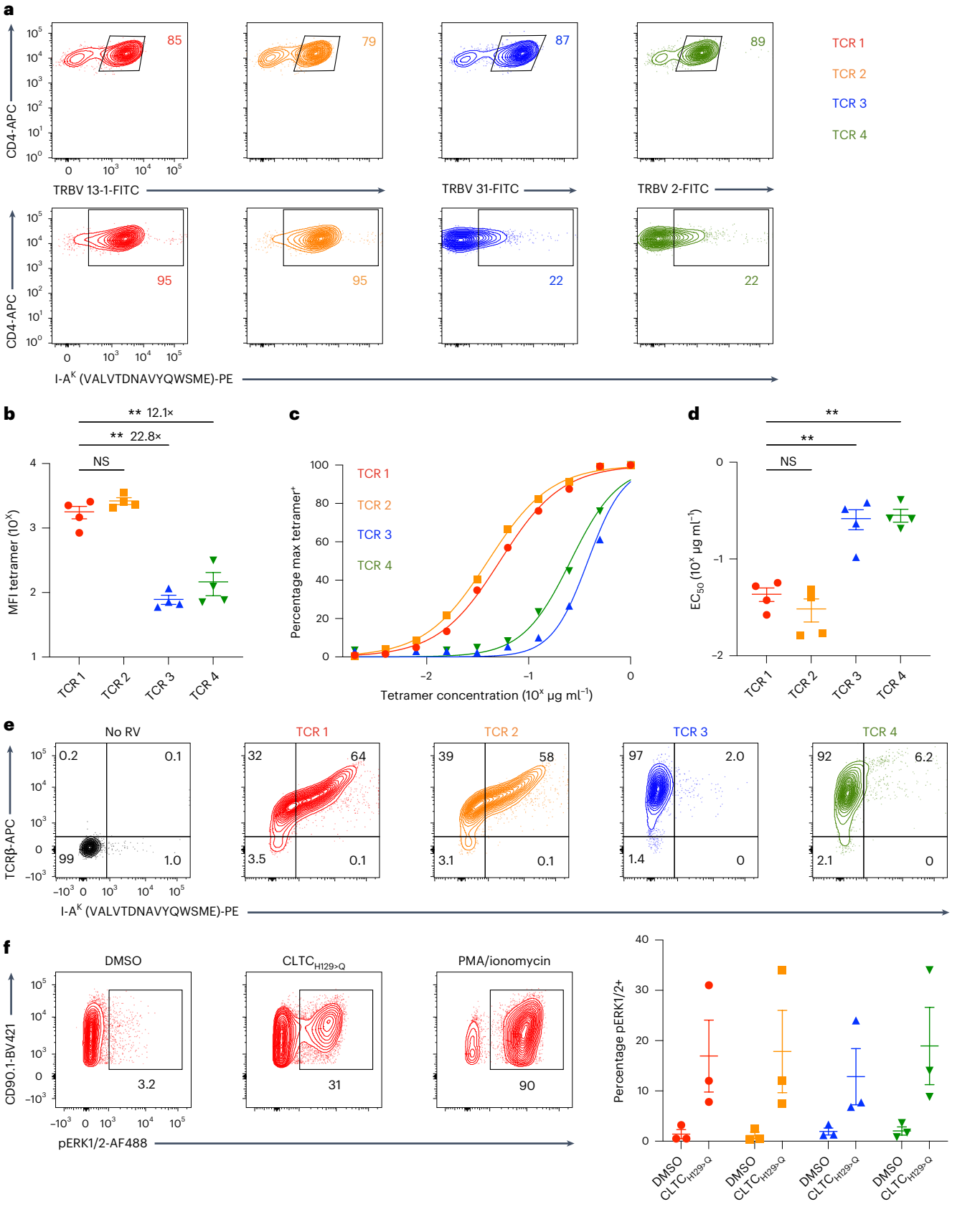

https://doi.org/10.1038/s41590-023-01543-9

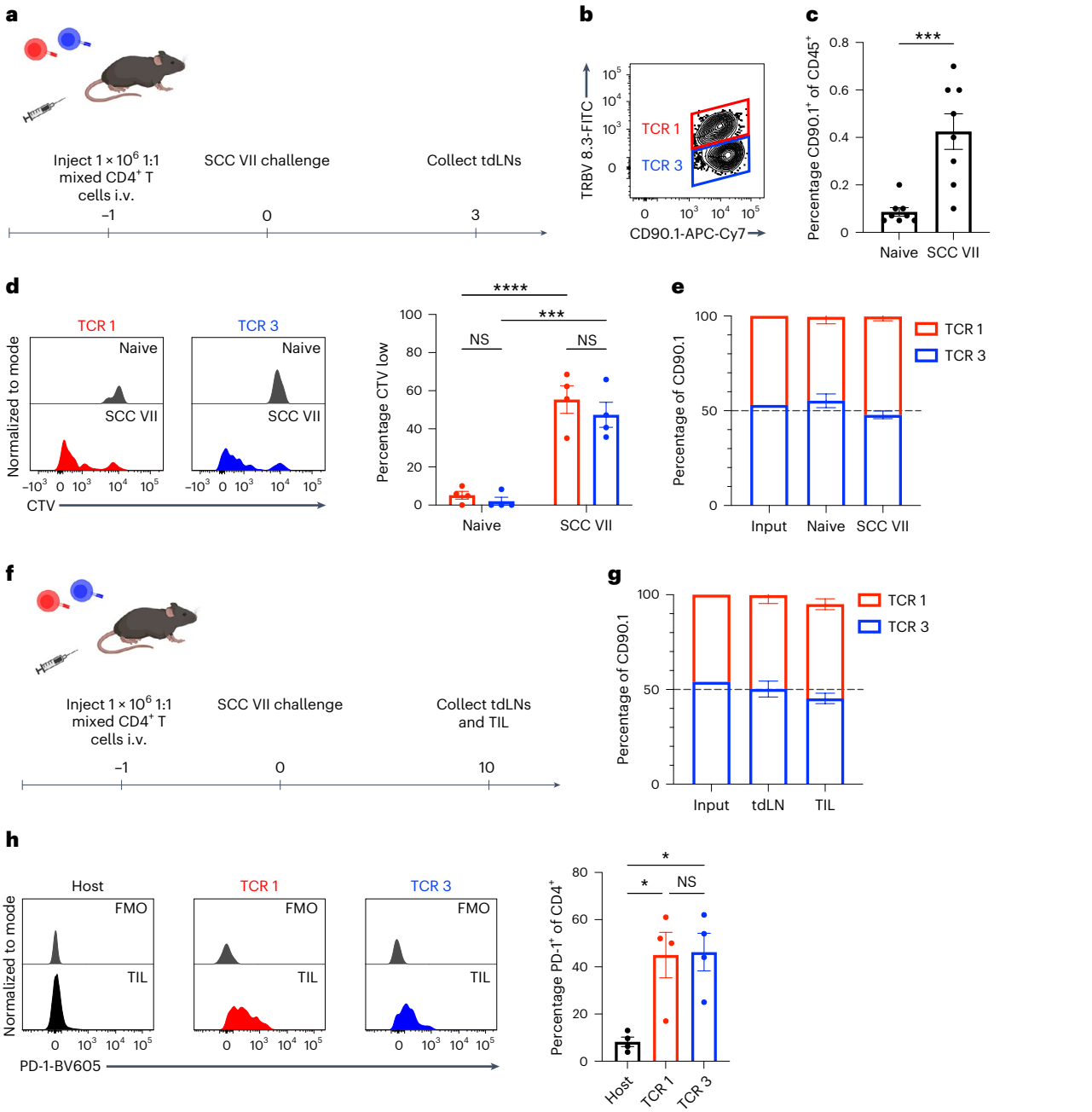

Fig. 3 | Expansion and activation of CLTC$_{H129>Q}$-specific CD4$^+$ T cells in the draining lymph node and tumor microenvironment is independent of TCR avidity. a, Schematic overview of co-transfer experiments performed for **c**–**e**. **b**, Representative flow cytometry plot demonstrating gating strategy to identify TCR 1- and TCR 3-expressing CD4$^+$ T cells in vivo. **c**, Quantification of total CD90.1$^+$ adoptively transferred CD4$^+$ T cells in draining lymph nodes of naive mice or mice challenged with SCC VII tumors; $n = 8$ mice per group; ***$P = 0.0006$ two-tailed unpaired t-test. Data represent two independent experiments. **d**, Flow cytometry histograms (left) and quantification (right) of CTV dilution by TCR 1- and TCR 3-expressing CD4$^+$ T cells in vivo in either naive mice or mice challenged with SCC VII tumors; $n = 4$ mice per group; ***$P = 0.0003$; ****$P = 0.00009$; two-way ANOVA with Šidák correction for multiple comparisons. Data are representative of two independent experiments. **e**, Relative frequencies of TCR 1- and TCR 3-expressing CD4$^+$ T cells in the draining lymph nodes of naive and tumor-bearing mice compared to input; $n = 4$ mice per group. **f**, Schematic overview of co-transfer experiments performed for **g**,**h**. **g**, Relative frequencies of TCR 1- and TCR 3-expressing CD4$^+$ T cells in the draining lymph nodes and TILs of tumor-bearing mice compared to input. $n = 4$ mice per group. **h**, Flow cytometry histograms (left) and quantification (right) of PD-1 expression by host CD4$^+$ T cells compared to T cells expressing either TCR 1 or TCR 3; $n = 4$ mice per group; *$P = 0.0153$ host versus TCR 1; $P = 0.0128$ host versus TCR 3; one-way ANOVA with Tukey correction for multiple comparisons. Data are representative of two independent experiments. All data are represented as mean ± s.e.m. FMO, Fluorescence Minus One Control.

activated CD4$^+$ T cells expressing the high avidity TCR 1 at 1 d before tumor challenge with SCC VII and green fluorescent protein (GFP) or luciferase (Luc) was sufficient to induce tumor rejection (Fig. 4b–d). This protection was antigen-specific, as mice receiving 3×10^6 activated polyclonal CD4$^+$ T cells not expressing the CLTC$_{H129>Q}$-specific TCR had tumor growth comparable to untreated mice. None of the five protected mice receiving a subsequent tumor challenge 30 d after initial rejection developed palpable tumors, suggesting the establishment

https://doi.org/10.1038/s41590-023-01543-9

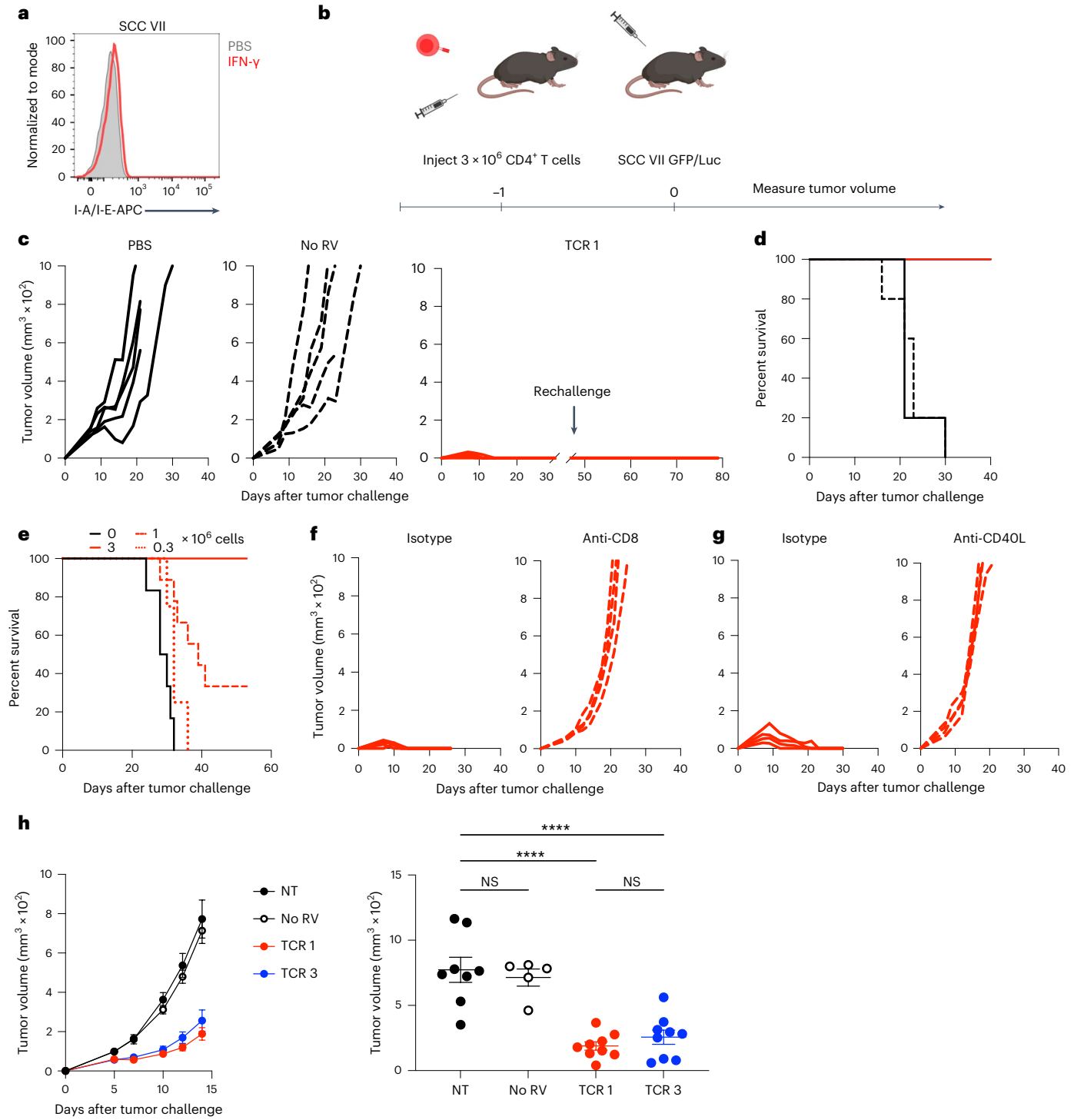

Fig. 4 | CLTC$_{H1290Q}$-specific CD4$^+$ T cells limit tumor burden in a CD8$^+$ T cell- and CD40L-dependent mechanism. a, Flow cytometry plots indicating surface expression of I-A^K/I-E^K molecules on SCC VII tumor cells in vitro after 48 h of culture in media supplemented with either phosphate-buffered saline (PBS) or 10 ng ml^{-1} IFN-γ. Data are representative of three independent experiments. **b**, Schematic of tumor protection experiments. **c**, Tumor growth curves for mice receiving PBS, 3 × 10^6 polyclonal mock transduced T cells or 3 × 10^6 TCR 1-expressing T cells intravenously (i.v.) 1 d before SCC VII-GFP/Luc tumor challenge. Data are representative of three independent experiments; $n = 5$ mice per group. **d**, Survival of mice shown in **c**. **e**, Survival of mice receiving the indicated number of T cells expressing TCR 1 before tumor challenge; $n = 4$ mice for 0.33 × 10^6; $n = 9$ for 1 × 10^6; $n = 8$ for 3 × 10^6 and $n = 6$ for not treated (NT). Data represent two independent experiments. **f**, Tumor growth curves for mice receiving 3 × 10^6 TCR 1-expressing T cells 1 d before SCC VII-GFP/Luc tumor challenge with concurrent injections of either anti-CD8 or isotype control antibodies; $n = 4$ mice for anti-CD8, $n = 5$ mice for isotype. Data are representative of two independent experiments. **g**, Tumor growth curves for mice receiving 3 × 10^6 TCR 1-expressing T cells 1 d before SCC VII-GFP/Luc tumor challenge with concurrent injections of either anti-CD40L or isotype control antibodies; $n = 4$ mice per group. Data are representative of two independent experiments. **h**, Tumor growth curves for mice receiving PBS, 3 × 10^6 polyclonal mock transduced T cells or 3 × 10^6 TCR 1- or TCR 3-expressing T cells i.v. 1 d before SCC VII tumor challenge (left). Tumor volumes at 14 d (right); $n = 8$ mice for untreated, $n = 5$ mice receiving no retrovirus (RV) mock transduced cells and $n = 9$ mice receiving cells expressing either TCR 1 or TCR 3. Data are representative of two independent experiments. ****$P = 0.00003$ for NT versus TCR 1; $P = 0.00006$ for NT versus TCR 3 two-way ANOVA with Šidák correction for multiple comparisons. Data are representative of two independent experiments. Data represent mean ± s.e.m.

of durable immune memory. Protection by $CLTC_{H129>Q}$-specific $CD4^+$ T cells was also dependent on the frequency of these cells at the time of tumor challenge, as mice receiving either 1×10^6 or 3.3×10^5 cells before challenge had decreased rates of survival after inoculation of SCC VII-GFP/Luc cells (Fig. 4e).

Given that SCC VII tumor cells do not express MHC-II (Fig. 4a), we reasoned that $CLTC_{H129>Q}$-specific $CD4^+$ T cell-mediated protection may be dependent on their role as helper cells for $CD8^+$ T cells[19]. Consistent with this, depletion of $CD8^+$ T cells before the transfer of $CD4^+$ T cells and tumor inoculation prevented tumor rejection (Fig. 4f). Recent work has demonstrated that $CD4^+$ T cells provide help to $CD8^+$ T cells by CD40L-dependent licensing of cDC1s during the primary tumor response[20]. Upon stimulation with $CLTC_{H129>Q}$ peptide-pulsed splenocytes in vitro, $CD4^+$ T cells expressing TCR 1 upregulated CD40L, suggesting that this mechanism may be responsible for protection from tumor challenge (Extended Data Fig. 3). To interrogate the role of this pathway in our model, we administered anti-CD40L-blocking antibodies on the day of tumor implantation and 2 d later. Mice receiving 3×10^6 activated $CLTC_{H129>Q}$-specific $CD4^+$ T cells along with anti-CD40L were no longer protected from tumor challenge (Fig. 4g). Together, these data demonstrate that NeoAg-specific $CD4^+$ T cells mediate antitumor immunity by helping endogenous $CD8^+$ T cells via CD40L signaling.

These findings prompted us to further probe the efficacy of $CD4^+$ T cells expressing either TCR 1 or TCR 3. As antitumor efficacy was dependent on CD40L help for $CD8^+$ T cells, we used the SCC VII parental cell line for all future experiments to rule out the contribution of $CD8^+$ T cells specific for epitopes contained within the GFP or Luc reporter proteins. While transfer of 3×10^6 cells expressing TCR 1 was no longer sufficient for complete tumor rejection against the less-immunogenic parental cell line, tumor growth was still significantly delayed compared to untreated mice or mice receiving 3×10^6 polyclonal activated $CD4^+$ T cells (Fig. 4h). There was no significant difference in the rate of tumor growth for mice receiving $CD4^+$ T cells expressing TCR 1 or TCR 3, however, suggesting that clones with differences in TCR avidity can mediate similar CD40L- and CD8-dependent antitumor functions in vivo.

TCR-engineered $CLTC_{H129>Q}$-specific $CD4^+$ T cells mediate therapeutic immunity

Given the observation that $CLTC_{H129>Q}$-specific $CD4^+$ T cells could contribute to primary tumor immunity, we investigated the potential of TCR-engineered T cells to limit tumor burden in the context of therapeutic ACT against large established tumors. In preliminary experiments, we found that ACT with $CD4^+$ T cells expressing TCR 1 did not significantly improve survival after tumor challenge compared to mice receiving non-transduced T cells, despite evidence that adoptively transferred cells were able to proliferate in the tdLNs and infiltrate tumors (Extended Data Fig. 4). We therefore sought to improve the function and survival of the engineered cells. Studies suggest that $CD8^+$ T cells primed under conditions that preferentially generate less-differentiated stem cell memory T (T_{SCM}) cells have a greater capacity for persistence and tumor destruction when adoptively transferred into tumor-bearing animals[21]. The common γ-chain cytokines IL-7 and IL-15 have been demonstrated to preferentially generate and expand T_{SCM}-like cells from ex vivo-stimulated, naive human $CD8^+$ T cells[22]. We therefore sought to determine whether culturing our TCR-engineered $CD4^+$ T cells in IL-7/IL-15, rather than IL-2, could generate T_{SCM}-like cells for ACT (Fig. 5a). $CD4^+$ T cells cultured in IL-7/IL-15 after TCR transduction demonstrated a significant increase in the frequency of $CD44^-CD62^+Sca\text{-}1^{hi}$ cells, consistent with a T_{SCM}-like phenotype (Fig. 5b and Extended Data Fig. 5a–d). Cells cultured in IL-7/IL-15 were also less proliferative in vitro compared to cells cultured in IL-2 (Extended Data Fig. 5e). Despite these differences in in vitro phenotype, the TCR transduction efficiency was comparable between both treatment groups as determined by CD90.1 expression (Extended Data Fig. 5f).

To compare the in vivo expansion and therapeutic efficacy of IL-7/IL-15-treated T_{SCM}-like cells with those cultured in IL-2, we transferred equal numbers (3×10^6) of TCR-engineered cells from either culture condition into mice with established SCC VII tumors 1 d following treatment with the lymphodepleting chemotherapy agent cyclophosphamide (Cy) (Fig. 5c). Notably, as soon as 4 d after transfer there was a roughly tenfold increase in the frequency of $CD90.1^+$ cells in the peripheral blood of mice receiving the IL-7/IL-15-treated cells, with this population peaking in size 9 d following adoptive transfer (Fig. 5d,e). Furthermore, animals receiving the T_{SCM}-like $CD4^+$ T cells had significantly delayed tumor growth compared to mice receiving the same number of T cells expanded in IL-2 (Fig. 5f). ACT with $CD4^+$ T cells cultured in IL-7/IL-15, but not IL-2, provided a significant increase in survival beyond the direct effects of the Cy chemotherapy (Fig. 5g). Consistent with our previous results, therapeutic ACT with T_{SCM}-like $CD4^+$ T cells expressing TCR 3 delayed tumor growth similarly to ACT with cells expressing TCR 1 (Fig. 5h,i). These results suggest that TCR-engineered NeoAg-specific $CD4^+$ T cells differentiated in IL-7/IL-15 can be effective as a therapeutic ACT treatment.

T_{SCM}-like $CLTC_{H129>Q}$-specific $CD4^+$ T cells are maintained in the tdLNs

To further investigate the cellular programs of therapeutic $CLTC_{H129>Q}$-specific T_{SCM}-like cells in vivo, $CD90.1^+CD4^+$ T cells were sorted from tdLNs and TILs 9 d after adoptive transfer of $CD4^+$ T cells expressing TCR 1 differentiated in either IL-2 or IL-7/IL-15. A significant increase in the frequency of $CD90.1^+CD4^+$ T cells was observed in both the tdLNs and TILs of mice receiving IL-7/IL-15-conditioned T cells compared to those cultured in IL-2, consistent with trends in the peripheral blood (Fig. 6a,b). Next, we performed bulk RNA sequencing (RNA-seq) to compare the transcriptomic features of cells treated with IL-2 or IL-7/IL-15 in these two tissue compartments. Principal-component analysis (PCA) revealed clustering of tdLN samples and TIL samples together, suggesting that the microenvironment promotes consistent transcriptomic features independent of cytokine treatment (Fig. 6c). To assess tissue-specific genetic signatures, we investigated differentially expressed genes between all TIL and tdLN samples regardless of cytokine treatment. Among genes differentially expressed in the tdLNs were *tcf7* and *sell*, markers of memory T cells, whereas cells from TILs expressed genes associated with effector functions, including type 1 helper T (T_H1) cytokines (*tnf*), TCR-signaling pathway components (*fos*) and cytotoxicity genes (*prf1*, *gzmc*, *gzme* and *gzmf*) (Fig. 6d). Therefore, we decided to further investigate the memory phenotypes of adoptively transferred cells in the tdLNs and TILs by flow cytometry. Consistent with our RNA-seq data, we identified memory subpopulations corresponding to effector memory (T_{EM}) cells ($CD44^+CD62L^-$), central memory T (T_{CM}) cells ($CD44^+CD62L^+$) and T_{SCM} cells ($CD44^-CD62L^+$) within the tdLNs (Fig. 6e). Notably, we identified a population of $CD90.1^+$ T_{SCM} cells within the lymph nodes of mice receiving cells treated with IL-7/IL-15 that was almost entirely absent in mice receiving IL-2-treated cells (Fig. 6f). In both groups, $CD90.1^+$ cells within the tumor were almost entirely of the T_{EM} phenotype, with little to no apparent expression of CD62L (Fig. 6g,h). These data suggest that adoptively transferred in vitro-generated T_{SCM} cells are selectively maintained as a reservoir in the tdLNs, where they give rise to more differentiated subsets capable of trafficking to the TME.

ACT with $CLTC_{H129>Q}$-specific $CD4^+$ T cells alters host $CD8^+$ T cell phenotypes

To determine whether therapeutically transferred $CLTC_{H129>Q}$-specific $CD4^+$ T cells are modulating $CD8^+$ T cell immunity, we investigated the phenotypes of $CD8^+$ T cells in the TILs and tdLNs of mice receiving therapeutic ACT. While Cy is lymphodepleting, other studies using a similar dose of the drug demonstrate that full lymphocyte recovery

https://doi.org/10.1038/s41590-023-01543-9

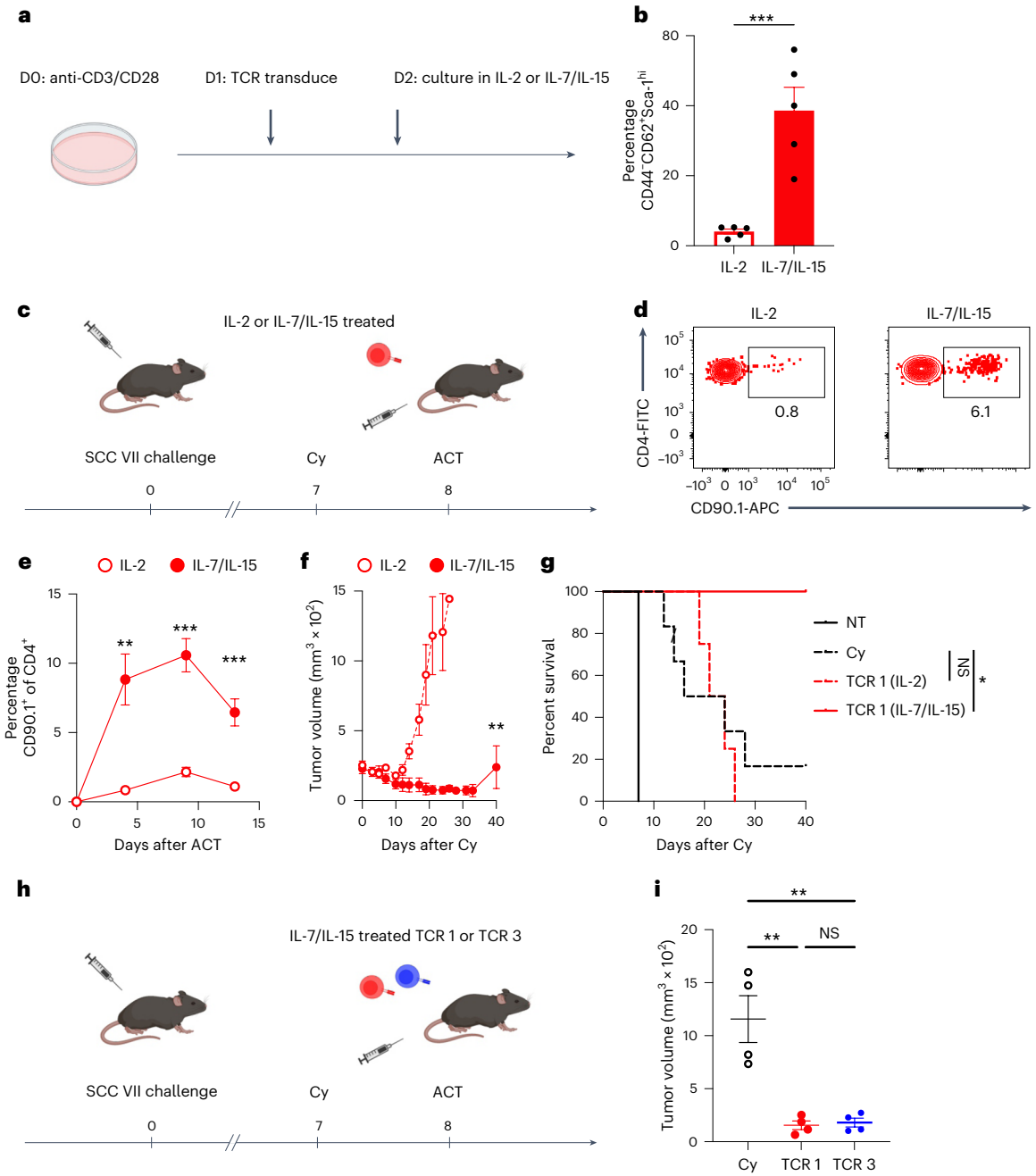

Fig. 5 | Therapeutic ACT with T_{SCM}-like $CLTC_{H129>Q}$-specific $CD4^+$ T cells promotes tumor control. a, Schematic of culture conditions to generate TCR-engineered T_{SCM}-like cells. **b**, Frequency of $CD44^-CD62L^+Sca\text{-}1^{hi}CD4^+$ T cells after culture with indicated cytokines. ***$P = 0.0009$; two-tailed unpaired *t*-test. Data represent five independent experiments. **c**, Schematic of therapeutic ACT experiments. **d**, Representative flow cytometry plots depicting frequency of $CD90.1^+$ adoptively transferred cells in the peripheral blood of mice 4 d after adoptive transfer. **e**, Quantification of $CD90.1^+$ adoptively transferred cells in the peripheral blood of mice over time after adoptive transfer. Data show mean ± s.e.m., $n = 4$ mice per group, and are representative of two independent experiments. **$P = 0.0051$; ***$P = 0.0002$ for day 9 and $P = 0.0003$ for day 13; two-tailed unpaired *t*-test. **f**, Tumor growth curves of mice treated with cyclophosphamide and 3×10^6 TCR 1-expressing cells from indicated treatment groups; $n = 4$ mice per group; **$P < 0.0077$; two-tailed unpaired *t*-test at day 21. **g**, Survival of mice in **d**. NS, $P = 0.74$; *$P = 0.025$; survival *P* values by log-rank test. **h**, Schematic of therapeutic ACT with TCR 1 or TCR 3-expressing cells. **i**, Tumor volumes of mice with indicated treatments 12 d after initiation of therapy; $n = 4$ mice per group; NS, $P = 0.99$; **$P = 0.0022$ Cy versus TCR 1; $P = 0.0025$ Cy versus TCR 3; two-way ANOVA with Šidák correction for multiple comparisons. All data represent mean ± s.e.m.

is apparent between 5–10 d following treatment[23,24], suggesting that endogenous host lymphocytes are available for interactions with adoptively transferred $CD4^+$ T cells. In the TME, there were no significant differences in the percentage of $CD8^+$ T cells expressing PD-1 (Fig. 7a,b). Given that higher levels of PD-1 expression correlate with terminally exhausted cell states[25], we also investigated the level of PD-1 expression by analyzing the MFI of PD-1^+CD8^+ T cells. We found that despite the similar absolute frequency of PD-1^+ cells, $CD8^+$ TILs from mice treated with T_{SCM}-like $CD4^+$ T cells cultured in IL-7/IL-15 expressed significantly lower levels of PD-1 compared to $CD8^+$ T cells from mice treated with Cy alone, suggesting that these $CD8^+$ T cells may be less terminally exhausted (Fig. 7c).

https://doi.org/10.1038/s41590-023-01543-9

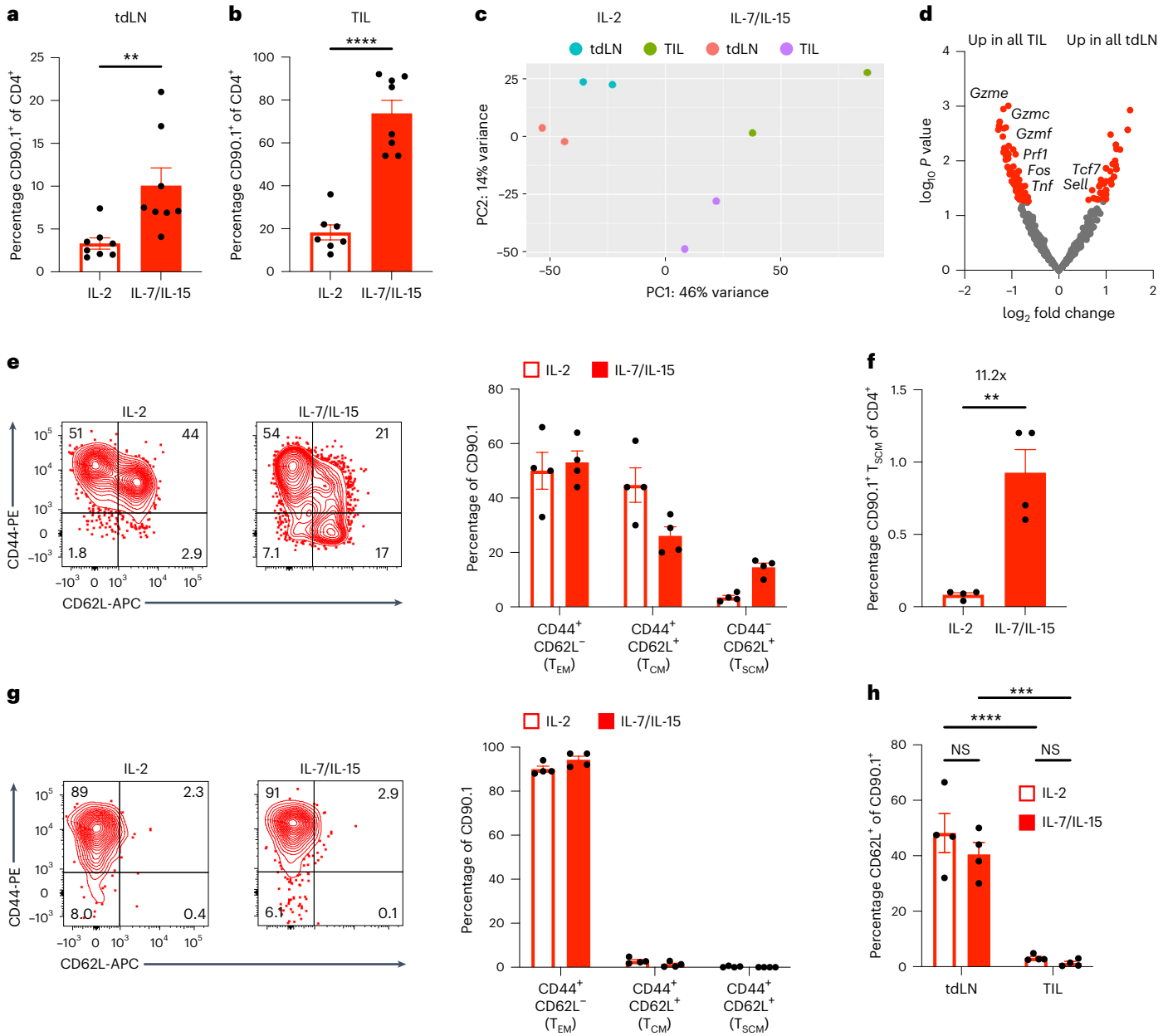

Fig. 6 | CD4$^+$ T_{SCM}-like cells are selectively maintained in the tumor-draining lymph nodes. a, Quantification of CD90.1$^+$ adoptively transferred cells in the tdLNs of mice 9 d following therapeutic ACT; $n = 8$ mice per group. Data represent two independent experiments; $^{**}P = 0.0074$; two-tailed unpaired t-test. **b**, Quantification of CD90.1$^+$ adoptively transferred cells in the TILs of mice 9 d following therapeutic ACT. $n = 8$ mice per group; data represent two independent experiments; $^{****}P = 0.00004$; two-tailed unpaired t-test. **c**, PCA plot depicting TIL- or tdLN-derived CD90.1$^+$ cells from either IL-2 or IL-7/IL-15 culture. **d**, Volcano plot highlighting differentially expressed genes between tdLN and TIL samples. $n = 4$ samples per group. P values were determined by the Wald test and adjusted for multiple tests using the Benjamini–Hochberg algorithm. Significant genes were considered as those with an adjusted P value < 0.05 and an absolute log fold change >1. **e**, Representative flow cytometry plots (left) and quantification (right) of T cell memory subsets present among CD90.1$^+$ cells in the tdLNs. $n = 4$ mice per group, representative of two independent experiments. **f**, Quantification of CD90.1$^+$ T_{SCM} present in tdLNs of mice receiving therapeutic ACT with either IL-2- or IL-7/IL-15-treated cells. $n = 4$ mice per group, representative of two independent experiments; $^{**}P = 0.0019$; two-tailed unpaired t-test. **g**, Representative flow cytometry plots (left) and quantification (right) of T cell memory subsets present among CD90.1$^+$ cells in TILs. $n = 4$ mice per group, representative of two independent experiments. **h**, Quantification of CD62L expression by CD90.1$^+$ T cells in the tdLNs or TILs of mice following therapeutic ACT. $n = 4$ mice per group, representative of two independent experiments; $^{***}P = 0.0001$; $^{****}P = 0.00003$; two-way ANOVA with Šidák correction for multiple comparisons. All data represented as mean ± s.e.m.

Given that CD4$^+$ T cell help for the priming of antigen-specific CD8$^+$ T cells is believed to occur in the local lymph nodes, we also investigated CD8$^+$ T cell phenotypes in the tdLNs of mice receiving therapy. Specifically, we again looked at PD-1 expression, which is known to correlate with stem-like, tumor-specific T cells in the tdLNs[26]. Notably, we found a significant increase in the frequency of PD-1$^+$CD8$^+$ T cells in the tdLNs of mice receiving adoptively transferred cells cultured in IL-7/IL-15 as compared to mice receiving cells cultured in IL-2 (Fig. 7d). Furthermore, there was a significant positive correlation between the frequency of CD90.1$^+$ adoptively transferred CD4$^+$ T cells and the frequency of PD-1$^+$CD8$^+$ T cells in lymph nodes from both IL-2 and IL-7/IL-15-treated mice (Fig. 7e). Overall, these data suggest that adoptively transferred

https://doi.org/10.1038/s41590-023-01543-9

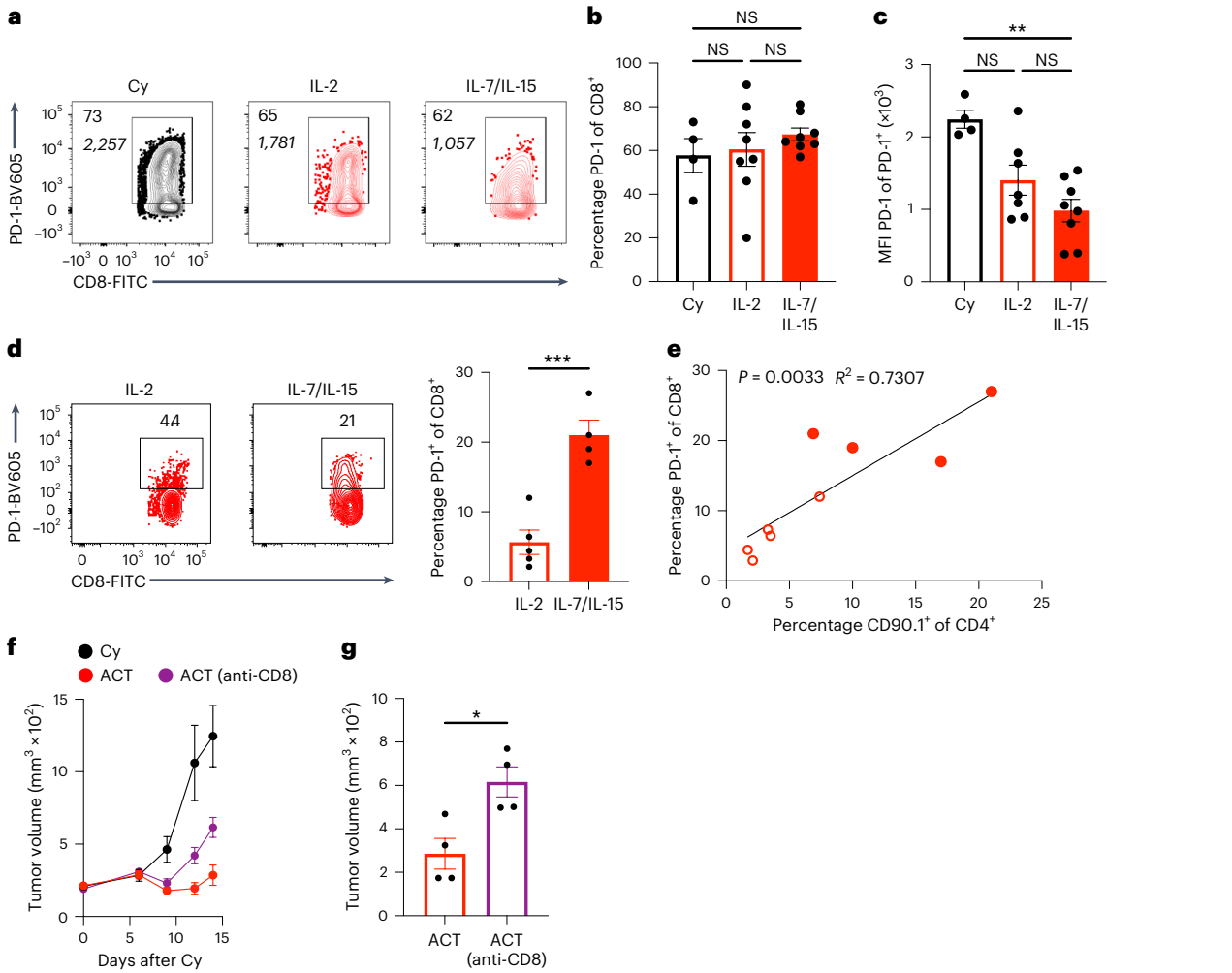

Fig. 7 | Therapeutic ACT with T_{SCM}-like $CLTC_{H129>Q}$-specific $CD4^+$ T cells requires host $CD8^+$ T cells. a, Representative flow cytometry plots indicating PD-1 expression by $CD8^+$ T cells from tumors collected 9 d after treatment with percentage (top) and MFI (bottom) indicated. **b**, Quantification of frequency of PD-1^+CD8^+ T cells from tumors. $n = 4$ mice for Cy treatment and $n = 8$ mice for IL-2 and IL-7/IL-15 ACT-treated groups. Data represent two independent experiments. NS, $P > 0.05$; two-way ANOVA. **c**, Quantification of PD-1 MFI of PD-1^+CD8^+ T cells from tumors. $n = 4$ mice for Cy treatment and $n = 8$ mice for IL-2 and IL-7/IL-15 ACT-treated group; data represent two independent experiments; $^{**}P = 0.0042$; two-way ANOVA with Šidák correction for multiple comparisons. **d**, Representative flow cytometry plots (left) and quantification (right) of PD-1^+CD8^+ T cells present in the tdLNs of mice receiving therapeutic ACT. $n = 5$ mice for IL-2 and $n = 4$ mice for IL-7/IL-15 groups, representative of two independent experiments. $^{***}P = 0.0008$; two-tailed unpaired t-test. **e**, Pearson correlation of the frequency of adoptively transferred CD90.1^+CD4^+ T cells versus the frequency of PD-1^+CD8^+ T cells in the tdLNs. $n = 5$ mice for IL-2 and 4 mice for IL-7/IL-15 groups, representative of two independent experiments. R^2 and two-tailed P value determined by Pearson correlation. **f**, Tumor growth curves of mice treated with cyclophosphamide ± 3×10^6 TCR 1-expressing cells treated with IL-7/IL-15 with or without CD8 depletion. $n = 4$ mice per group. Data are representative of two independent experiments. **g**, Tumor volumes from treated mice from **f** 14 d following treatment with or without CD8 depletion. $^*P = 0.0014$ two-tailed unpaired t-test. All data represent mean ± s.e.m.

T_{SCM}-like $CD4^+$ T cells recognizing $CLTC_{H129>Q}$ are actively involved in the priming of tumor-specific $CD8^+$ T cells in the tdLNs.

To confirm the role of host $CD8^+$ T cells in therapeutic ACT experiments, we treated mice with IL-7/IL-15-treated $CD4^+$ T cells expressing TCR 1 with or without concurrent antibody-mediated depletion of $CD8^+$ T cells. While initially, following treatment, CD8-depleted mice exhibited delayed tumor growth compared to mice treated with Cy alone, ultimately CD8-depleted mice had significantly increased tumor burden relative to treated mice without depletion (Fig. 7f,g). These results confirm that endogenous host $CD8^+$ T cells are required for therapeutic efficacy of ACT with $CLTC_{H129Q}$-specific $CD4^+$ T cells.

Discussion

In this study we have analyzed an oligoclonal $CD4^+$ T cell response to a naturally arising tumor NeoAg at the level of TCR usage and functionality. Although there has been a greater emphasis on $CD8^+$ T cell responses in this context, perhaps due to the fact that they can directly recognize most tumors and the comparative ease in identifying the target NeoAgs presented by MHC-I versus MHC-II, the fact that $CD4^+$ T cells are crucial for the priming and regulation of $CD8^+$ T cells suggests that a deeper understanding of their response to cancer could significantly improve existing immunotherapies, including ACT. In this study, we investigated how differences in TCR characteristics and T cell functional states impact the efficacy of ACT with NeoAg-specific $CD4^+$ T cells.

Cloning multiple $CLTC_{H129>Q}$-specific TCRs from SCC VII-immune mice allowed us to investigate how TCR-binding kinetics may impact T cell-intrinsic and extrinsic factors contributing to the antitumor immune response. We demonstrate that while $CLTC_{H129>Q}$-specific TCR 3 has a comparatively lower avidity for peptide–MHC complexes than

TCR 1, CD4$^+$ T cells expressing either TCR are similarly able to transduce TCR signaling, proliferate in vivo, contribute to CD8$^+$ T cell- and CD40L-dependent primary tumor immunity and provide therapeutic tumor control. These data suggest that across the range investigated in this study, TCR avidity does not significantly affect cell-intrinsic TCR signaling or cell-extrinsic interactions providing CD40L stimulation to accessory antigen-presenting cells (APCs), as is likely required for effective licensing of dendritic cells and subsequent priming of CD8$^+$ T cells in our model. These results are consistent with studies in chronic infection models suggesting that tetramer-binding avidity may not correlate with CD4$^+$ T cell function or fate. Specifically, a study of lymphocytic choriomeningitis virus infection in mice found that tetramer-negative low affinity CD4$^+$ T cells exist at a similar frequency to tetramer-positive cells and contribute inflammatory cytokines during the effector phase[27]. Other studies suggest that the off-rate (K^{off}) of TCR interactions with peptide–MHC complexes may play a role in the commitment of individual clonotypes to distinct T_H cell and memory lineages, whereas TCR avidity as measured by tetramer-binding studies alone did not correlate with either[28,29]. Notably, recent studies of MHC-I-restricted TCRs recognizing tumor antigens with a similar range of tetramer-binding capacity to those in our study did observe a correlation between TCR avidity and T cell functions in vitro and in vivo, suggesting that the possibility that CD4$^+$ and CD8$^+$ T cell subsets and their respective functions have different TCR avidity requirements[18,30]. One limitation of our study is the requirement for T cell activation before TCR expression by retroviral transduction; we were therefore unable to determine whether TCR avidity differentially regulates T cell activation and priming of naive T cells during primary tumor immunity. Furthermore, the TCRs identified in this study were isolated from polyclonal CD4$^+$ T cells following tumor rejection, likely reflecting a memory population; TCRs collected from the effector phase during tumor growth may have more diverse functional properties.

It is notable that SCC VII tumor cells do not express MHC-II, even after treatment with IFN-γ. While transcriptomic signatures corresponding to cytotoxic CD4$^+$ T cells have been identified in patients with melanoma and bladder cancer[31,32] and direct tumor recognition by CD4$^+$ T cells has been observed[33,34], studies also suggest that only a small subset of melanomas harbor any MHC-II$^+$ cells[35]. Even among MHC-II$^+$ tumor cells, endogenous antigens are selectively presented by MHC-II, which may limit direct recognition of critical tumor NeoAg[36]. A recent study from Rosenberg and colleagues demonstrated that among 20 confirmed NeoAg-specific TCRs isolated from CD4$^+$ TILs found in human tumors, none was able to directly recognize autologous tumor cells[37]. Despite the inability of SCC VII cells to express MHC-II, cells expressing TCR 1 within the TME were enriched for transcripts associated with cytotoxicity (*prf1*, *gzmc*, *gzme* and *gzmf*), suggesting that this transcriptomic signature may be broadly associated with local CD4$^+$ effector T cell differentiation even in cases where such cells cannot directly engage tumor cells. Overall, MHC-II$^-$ solid tumor models such as SCC VII may more closely model human disease and are an important alternative to murine cancer cells with inducible or constitutive MHC-II expression.

While SCC VII cells do not express MHC-II, ACT with T_{SCM}-like TCR-engineered CD4$^+$ T cells generates effective therapeutic immunity in the context of established solid tumors that is dependent on CD8$^+$ T cells and likely mediated by APC activation ('licensing') via CD40/CD40L interactions[38]. Several studies now implicate migratory cDC1 as the recipient of CD40L stimulation from CD4$^+$ T cells in humans and mice[20,39,40], suggesting that these are the relevant APC in our study. Consistent with our hypothesis of improved CD8$^+$ T cell priming, we observed a significant increase in the frequency of PD-1$^+$ CD8$^+$ T cells in the tdLNs during effective therapeutic ACT. In addition, CD8$^+$ TILs in mice treated with T_{SCM}-like CD4$^+$ T cells expressed lower levels of PD-1 in the TME, consistent with previously published results suggesting that CD8$^+$ T cells primed in the absence of help express higher levels of co-inhibitory receptors[41]. While our results implicate a role for T cell help in the tdLNs, we cannot rule out additional cooperative functions locally within the TME between newly primed CD8$^+$ T cells and NeoAg-specific CD4$^+$ T cells, such as CD4$^+$ T cell-derived IL-2 and IFN-γ, which serve to support CD8$^+$ T cell survival in and recruitment to tumors, respectively[42]. Indeed, our data suggest that adoptively transferred CD4$^+$ T cells are also capable of recognizing antigen in the TME, where they express a transcriptomic signature associated with effector function and differentiation. In addition, given that CD8$^+$ T cell depletion does not completely abrogate antitumor efficacy in our therapeutic models, it is likely that additional mechanisms beyond APC licensing, such as local effector cytokine secretion, are required.

To improve the persistence of adoptively transferred CD4$^+$ T cells, we administered Cy as a lymphodepletion regimen before ACT. In addition to depleting inhibitory lymphocytes and increasing homeostatic cytokine levels, lymphodepleting regimens have been reported to promote the release of innate immune ligands such as lipopolysaccharide (LPS) from gut microbiota, which potentiates host dendritic cell activation[43]. Notably, C3H/HeJ mice have a missense mutation in TLR4, which likely reduces the impact of this signaling axis following lymphodepletion and may therefore underestimate the efficacy of Cy in our model.

The superior efficacy of IL-7/IL-15-treated CD4$^+$ T cells merits further investigation. While previous studies have demonstrated an enhanced capacity for expansion and therapeutic efficacy of CD4$^+$ T cells primed in the presence of IL-7 or expressing a constitutively active mutant of STAT5 (refs. 44,45), our study extends these findings by demonstrating that IL-7/IL-15-treated CD4$^+$ T cells adopt a unique surface phenotype in vitro associated with T_{SCM}-like cells, which has mainly described in the context of tumor-specific CD8$^+$ T cells. Other cytokines and treatments, such as IL-21, IL-9 and Wnt pathway inhibitors, have been described as inducers of T_{SCM}-like CD8$^+$ T cells and may similarly promote this phenotype in CD4$^+$ T cells[21,46,47]. While IL-7 and IL-15 were used at a single concentration in our study, it is possible that altering the concentration of these cytokines may improve the yield of T_{SCM}-like cells in this context. Our data demonstrate that following adoptive transfer, TCR-engineered T_{SCM}-like cells generated in culture with IL-7/IL-15 maintain a reservoir in the tdLNs accounting for nearly a quarter of all CD90.1$^+$ cells, whereas tumor-infiltrating cells express a differentiated effector memory phenotype. Several recent studies have highlighted the tdLNs as a crucial site for the maintenance of CD8$^+$ tumor-specific T cells expressing memory-associated features, which seem critical for responses to ICB[26,48,49]. Our results suggest that these tdLN-resident memory cell populations may be effectively installed via ACT in patients lacking a sufficient tumor-specific memory cell reservoir and highlight the potential for combination therapies with ICB.

ACT with NeoAg-specific CD4$^+$ T cells may have important advantages over ACT with CD8$^+$ T cells. First, studies suggest that in both murine models and human cancers, NeoAg-specific CD4$^+$ T cells may be more abundant than NeoAg-specific CD8$^+$ T cells. In preclinical and clinical studies of personalized cancer vaccines, epitopes selected for binding to MHC-I perhaps surprisingly predominantly gave rise to CD4$^+$ T cell responses[6,50]. In our own functional NeoAg screening approach applied to SCC VII, which does not leverage bioinformatic MHC binding predictions, we identified four MHC-II-restricted NeoAg and only one MHC-I-restricted NeoAg following vaccination with irradiated tumor cells[16]. This suggests that there may be a relative abundance of MHC-II-restricted TCRs available for immunotherapy, including previously identified TCRs specific for shared oncogenic driver mutations such as BRAF V600E[11], KRAS G12V[36,51] and G12D[4] and IDH1 R132H[52]. In addition, by operating independently of direct tumor recognition, such as by marshaling a polyclonal CD8$^+$ T cell response, ACT with CD4$^+$ T cells may circumvent immune escape mechanisms associated with monoclonal CD8$^+$ T cell ACT[53,54]. Overall, our study demonstrates the

efficacy of ACT with NeoAg-specific CD4$^+$ T cells in a physiologically relevant tumor model and brings new insights to the use of similar approaches for adoptive immunotherapy of human cancer to empower more diverse, potent and durable antitumor immune responses.

Online content

Any methods, additional references, Nature Portfolio reporting summaries, source data, extended data, supplementary information, acknowledgements, peer review information; details of author contributions and competing interests; and statements of data and code availability are available at https://doi.org/10.1038/s41590-023-01543-9.

References

1. Linnemann, C. et al. High-throughput epitope discovery reveals frequent recognition of neo-antigens by CD4$^+$ T cells in human melanoma. *Nat. Med.* **21**, 81–85 (2015).
2. Oliveira, G. et al. Phenotype, specificity and avidity of antitumour CD8$^+$ T cells in melanoma. *Nature* **596**, 119–125 (2021).
3. Malekzadeh, P. et al. Antigen experienced T cells from peripheral blood recognize p53 neoantigens. *Clin. Cancer Res.* **26**, 1267–1276 (2020).
4. Cafri, G. et al. Memory T cells targeting oncogenic mutations detected in peripheral blood of epithelial cancer patients. *Nat. Commun.* **10**, 449 (2019).
5. Snyder, A. et al. Genetic basis for clinical response to CTLA-4 blockade in melanoma. *N. Engl. J. Med.* **371**, 2189–2199 (2014).
6. Ott, P. A. et al. An immunogenic personal neoantigen vaccine for patients with melanoma. *Nature* **547**, 217–221 (2017).
7. Ott, P. A. et al. A phase Ib trial of personalized neoantigen therapy plus anti-PD-1 in patients with advanced melanoma, non-small cell lung cancer, or bladder cancer. *Cell* **183**, 347–362 (2020).
8. Keskin, D. B. et al. Neoantigen vaccine generates intratumoral T cell responses in phase Ib glioblastoma trial. *Nature* **565**, 234–239 (2019).
9. Tran, E. et al. Cancer immunotherapy based on mutation-specific CD4$^+$ T cells in a patient with epithelial cancer. *Science* **344**, 641–645 (2014).
10. Lu, Y.-C. et al. Treatment of patients with metastatic cancer using a major histocompatibility complex class II–restricted T-cell receptor targeting the cancer germline antigen MAGE-A3. *J. Clin. Oncol.* **35**, 3322–3329 (2017).
11. Veatch, J. R. et al. Tumor-infiltrating BRAF V600E -specific CD4$^+$ T cells correlated with complete clinical response in melanoma. *J. Clin. Invest.* **128**, 1563–1568 (2018).
12. Veatch, J. R. et al. Neoantigen-specific CD4$^+$ T cells in human melanoma have diverse differentiation states and correlate with CD8$^+$ T cell, macrophage, and B cell function. *Cancer Cell* **40**, 393–409 (2022).
13. Quezada, S. A. et al. Tumor-reactive CD4$^+$ T cells develop cytotoxic activity and eradicate large established melanoma after transfer into lymphopenic hosts. *J. Exp. Med.* **207**, 637–650 (2010).
14. Haabeth, O. A. W. et al. CD4$^+$ T cell-mediated rejection of MHC class II-positive tumor cells is dependent on antigen secretion and indirect presentation on host APCs. *Cancer Res.* **78**, 4573–4585 (2018).
15. Brightman, S. E., Naradikian, M. S., Miller, A. M. & Schoenberger, S. P. Harnessing neoantigen specific CD4 T cells for cancer immunotherapy. *J. Leukoc. Biol.* **107**, 625–633 (2020).
16. Dolina, J. S. et al. Linked CD4$^+$/CD8$^+$ T cell neoantigen vaccination overcomes immune checkpoint blockade resistance and enables tumor regression. Preprint at *bioRxiv* https://doi.org/10.1101/2023.05.06.539290 (2023).
17. Dash, P., Wang, G. C. & Thomas, P. G. Single-cell analysis of T-cell receptor repertoire. *Methods Mol. Biol.* **1343**, 181–197 (2015).
18. Zhong, S. et al. T-cell receptor affinity and avidity defines antitumor response and autoimmunity in T-cell immunotherapy. *Proc. Natl Acad. Sci. USA* **110**, 6973–6978 (2013).
19. Borst, J., Ahrends, T., Bąbała, N., Melief, C. J. M. & Kastenmüller, W. CD4$^+$ T cell help in cancer immunology and immunotherapy. *Nat. Rev. Immunol.* **18**, 635–647 (2018).
20. Ferris, S. T. et al. cDC1 prime and are licensed by CD4$^+$ T cells to induce anti-tumour immunity. *Nature* **584**, 624–629 (2020).
21. Gattinoni, L. et al. Wnt signaling arrests effector T cell differentiation and generates CD8$^+$ memory stem cells. *Nat. Med.* **15**, 808–813 (2009).
22. Cieri, N. et al. IL-7 and IL-15 instruct the generation of human memory stem T cells from naive precursors. *Blood* **121**, 573–584 (2013).
23. Salem, M. L. et al. Recovery from cyclophosphamide-induced lymphopenia results in expansion of immature dendritic cells which can mediate enhanced prime-boost vaccination antitumor responses in vivo when stimulated with the TLR3 agonist poly(I:C). *J. Immunol.* **182**, 2030–2040 (2009).
24. Ding, Z. C., Blazar, B. R., Mellor, A. L., Munn, D. H. & Zhou, G. Chemotherapy rescues tumor-driven aberrant CD4$^+$ T-cell differentiation and restores an activated polyfunctional helper phenotype. *Blood* **115**, 2397–2406 (2010).
25. Wherry, E. J. & Kurachi, M. Molecular and cellular insights into T cell exhaustion. *Nat. Rev. Immunol.* **15**, 486–499 (2015).
26. Huang, Q. et al. The primordial differentiation of tumor-specific memory CD8$^+$ T cells as bona fide responders to PD-1/PD-L1 blockade in draining lymph nodes. *Cell* **185**, 4049–4066 (2022).
27. Sabatino, J. J., Huang, J., Zhu, C. & Evavold, B. D. High prevalence of low affinity peptide-MHC II tetramer-negative effectors during polyclonal CD4$^+$ T cell responses. *J. Exp. Med.* **208**, 81–90 (2011).
28. Tubo, N. J. et al. Single naive CD4$^+$ T cells from a diverse repertoire produce different effector cell types during infection. *Cell* **153**, 785–796 (2013).
29. Kim, C., Wilson, T., Fischer, K. F. & Williams, M. A. Sustained interactions between T cell receptors and antigens promote the differentiation of CD4$^+$ memory T cells. *Immunity* **39**, 508–520 (2013).
30. Purcarea, A. et al. Signatures of recent activation identify a circulating T cell compartment containing tumor-specific antigen receptors with high avidity. *Sci. Immunol.* **7**, eabm2077 (2022).
31. Oh, D. Y. et al. Intratumoral CD4$^+$ T cells mediate anti-tumor cytotoxicity in human bladder cancer. *Cell* **181**, 1612–1625 (2020).
32. Cachot, A. et al. Tumor-specific cytolytic CD4 T cells mediate protective immunity against human cancer. *Sci. Adv.* https://doi.org/10.1126/sciadv.abe3348 (2021).
33. Yao, X. et al. Isolation and characterization of an HLA-DPB1*04:01-restricted MAGE-A3 T-cell receptor for cancer immunotherapy. *J. Immunother.* **39**, 191–201 (2016).
34. Oliveira, G. et al. Landscape of helper and regulatory CD4$^+$ T cells in melanoma. *Nature* **9**, A684 (2022).
35. Rodig, S. J. et al. MHC proteins confer differential sensitivity to CTLA-4 and PD-1 blockade in untreated metastatic melanoma. *Sci. Transl. Med.***10**, eaar3342 (2018).
36. Brightman, S. E. et al. Tumor cells fail to present MHC-II restricted epitopes derived from oncogenes to CD4$^+$ T cells. *JCI Insight* https://doi.org/10.1172/jci.insight.165570 (2022).
37. Lowery, F. J. et al. Molecular signatures of antitumor neoantigen-reactive T cells from metastatic human cancers. *Science* **375**, 877–884 (2022).
38. Schoenberger, S. P., Toes, R. E., van der Voort, E. I., Offringa, R. & Melief, C. J. T-cell help for cytotoxic T lymphocytes is mediated by CD40–CD40L interactions. *Nature* **393**, 480–483 (1998).
39. Wu, R. et al. Mechanisms of CD40-dependent cDC1 licensing beyond costimulation. *Nat. Immunol.* **23**, 1536–1550 (2022).

40. Lei, X. et al. CD4+ helper T cells endow cDC1 with cancer-impeding functions in the human tumor micro-environment. *Nat. Commun.* **14**, 217 (2023).
41. Ahrends, T. et al. CD4+ T cell help confers a cytotoxic t cell effector program including coinhibitory receptor downregulation and increased tissue invasiveness. *Immunity* **47**, 848–861 (2017).
42. Bos, R. & Sherman, L. A. CD4+ T-cell help in the tumor milieu is required for recruitment and cytolytic function of CD8+ T lymphocytes. *Cancer Res.* **70**, 8368–8377 (2010).
43. Paulos, C. M. et al. Microbial translocation augments the function of adoptively transferred self/tumor-specific CD8+ T cells via TLR4 signaling. *J. Clin. Invest.* **117**, 2197–2204 (2007).
44. Ding, Z.-C. et al. Persistent STAT5 activation reprograms the epigenetic landscape in CD4+ T cells to drive polyfunctionality and antitumor immunity. *Sci. Immunol.* **5**, eaba5962 (2020).
45. Ding, Z. C. et al. IL-7 signaling imparts polyfunctionality and stemness potential to CD4+ T cells. *OncoImmunology* **5**, e1171445 (2016).
46. Li, Y. et al. Targeting IL-21 to tumor-reactive T cells enhances memory T cell responses and anti-PD-1 antibody therapy. *Nat. Commun.* **12**, 951 (2021).
47. Kalbasi, A. et al. Potentiating adoptive cell therapy using synthetic IL-9 receptors. *Nature* **607**, 360–365 (2022).
48. Connolly, K. A. et al. A reservoir of stem-like CD8+ T cells in the tumor-draining lymph node preserves the ongoing anti-tumor immune response. *Sci. Immunol.* **7836**, 31–40 (2021).
49. Schenkel, J. M. et al. Conventional type I dendritic cells maintain a reservoir of proliferative tumor-antigen specific TCF-1+CD8+ T cells in tumor-draining lymph nodes. *Immunity* **54**, 2338–2353 (2021).
50. Kreiter, S. et al. Mutant MHC class II epitopes drive therapeutic immune responses to cancer. *Nature* **520**, 692–696 (2015).
51. Veatch, J. R. et al. Endogenous CD4+ T cells recognize neoantigens in lung cancer patients, including recurrent oncogenic KRAS and ERBB2 (Her2) driver mutations. *Cancer Immunol. Res.* **2**, 910–922 (2019).
52. Platten, M. et al. A vaccine targeting mutant IDH1 in newly diagnosed glioma. *Nature* **592**, 463–468 (2021).
53. Nagarsheth, N. B. et al. TCR-engineered T cells targeting E7 for patients with metastatic HPV-associated epithelial cancers. *Nat. Med.* **27**, 419–425 (2021).
54. Tran, E. et al. T-cell transfer therapy targeting mutant KRAS in cancer. *N. Engl. J. Med.* **375**, 2255–2262 (2016).

Spencer E. Brightman[1,2], Angelica Becker[1], Rukman R. Thota[1], Martin S. Naradikian[1], Leila Chihab[3], Karla Soria Zavala[1], Ashmitaa Logandha Ramamoorthy Premlal[3], Ryan Q. Griswold[1,2], Joseph S. Dolina[1], Ezra E. W. Cohen[4], Aaron M. Miller[1,4], Bjoern Peters[4,5] & Stephen P. Schoenberger[1]

[1]Division of Developmental Immunology, La Jolla Institute for Immunology, La Jolla, CA, USA. [2]Biomedical Sciences Program, School of Medicine, University of California San Diego, La Jolla, CA, USA. [3]Division of Vaccine Discovery, La Jolla Institute for Immunology, La Jolla, CA, USA. [4]Division of Hematology and Oncology, University of California San Diego Moores Cancer Center, UCSD, La Jolla, CA, USA. [5]Department of Medicine, University of California San Diego, La Jolla, CA, USA. e-mail: sps@lji.org

Methods

Animals

Female C3H/HeJ mice (The Jackson Laboratory) were used in these experiments. Animals were 8–12 weeks of age and maintained/bred in The La Jolla Institute for Immunology vivarium under specific-pathogen-free conditions in accordance with guidelines of the Association for Assessment and Accreditation of Laboratory Animal Care International and animal studies were approved by The La Jolla Institute for Immunology Institutional Animal Care and Use Committee.

Cell culture

The squamous cell carcinoma VII San Francisco line (SCC VII) spontaneously arose from the abdominal wall of a C3H mouse in the laboratory of Herman Suit (Harvard University) and was adapted for partial in vitro growth by K.K. Fu and K.N. Lam (University of California). SCC VII was maintained for a maximum of three passages in vitro in RPMI 1640 medium containing 10% fetal bovine serum (FBS) and penicillin–streptomycin (100 U ml^{-1} each, Gibco). To regenerate SCC VII P_0 cells, C3H/HeJ mice were subcutaneously (s.c.) injected with 5×10^5 cells in 1× HBSS and tumors were collected 14 d after inoculation. Tumor tissue was dissociated with a mouse Tumor Dissociation kit (Miltenyi Biotec) followed by passage through a 70-µm cell strainer (Fisher Scientific) and homogenized cells were re-seeded in vitro. For generation of SCC VII expressing luciferase and copepod-derived GFP (SCC VII-Luc/GFP), cells were transduced with the BVLIV713VA-1 HIV lentiviral vector (System Biosciences) under 10 µg ml^{-1} puromycin selection and further purified using GFP + FACS-sorting. The $58\alpha^-\beta^-$ hybridoma cell line was cultured in RPMI medium supplemented with L-glutamine and HEPES (10 mM, Gibco), 10% FBS, 1 mM sodium pyruvate (Gibco), 1× MEM Non-Essential Amino Acids (Gibco) and penicillin–streptomycin (100 U ml^{-1} each, Gibco).

Whole-cell vaccination and tumor challenge

Whole tumor cell vaccination experiments were conducted via s.c. injection of 10×10^6 50 Gy-irradiated SCC VII cells in 1× HBSS with 50 µg polyI:C (Thermo Fisher). Immunized mice were challenged 14 d later by s.c. injection of 5×10^5 live SCC VII cells.

Preparation of single-cell suspensions

Spleens, inguinal lymph nodes and tumors were surgically removed at experiment end points. Spleens were dissociated manually and cell suspensions were passed through a 70-µm strainer. Before use as APCs in in vitro assays, red blood cells were lysed with ACK lysis buffer (Thermo Fisher). Inguinal lymph nodes and subcutaneous tumors were minced into small (<2 mm) pieces with dissection scissors. Tissue fragments were enzymatically dissociated in 20 µg ml^{-1} Liberase (Roche) and 20 µg ml^{-1} DNase I (Roche) at 37 °C for 30 min. Single cells were passed through a 70-µm strainer.

TCR sequencing

Single tetramer-positive $CD4^+$ T cells from the spleens of SCC VII-immune mice 14 d after challenge were sorted into 96-well plates using an FACS Fusion (BD). Multiplexed PCR amplification of the TCR α and α variable regions was performed as previously described[17]. cDNA libraries were sequenced by Sanger sequencing (ETON). Full-length TCR sequences were reconstructed from cDNA fragments using the IMGT database to identify corresponding V and J gene usage[55]. IMGT nomenclature for TCR V and J genes is used throughout the manuscript for consistency.

TCR cloning and expression

TCR nucleotide sequences were synthesized and cloned into MSGV1 retroviral expression backbones using a BioXP (Codex DNA). TCR β and α-chains were separated by a P2A ribosomal skipping element. For in vivo studies, constructs were synthesized encoding the TCR β and α-chains as described above, followed by an additional P2A sequence and the coding sequence of CD90.1. Spleens from naive C3H/Hej mice were dissociated manually and cell suspensions passed through a 70-µm filter. $CD4^+$ T cells were isolated by magnetic negative selection (StemCell). $CD4^+$ T cells were stimulated with anti-CD3/CD28 Dynabeads (Gibco) for 24 h. TCR retroviral supernatants were generated by co-transfection of Platinum-Eco cells with the TCR containing retroviral vectors and pcL-ECo plasmid. Retroviral supernatants were collected at 48 and 72 h after transfection and either used fresh or frozen at −80 °C. Transductions were performed on RetroNectin-coated plates (Takara) as previously described. Murine T cells were maintained in RPMI 1640 supplemented with 10% FBS, 50 µM β-mercaptoethanol, 1× penicillin–streptomycin and HEPES supplemented with 100 IU ml^{-1} human IL-2 (Roche) or 5 ng ml^{-1} human IL-7 and IL-15 (StemCell) in the presence of anti-CD3/CD28 Dynabeads (Thermo Fisher) for expansion and used for experiments between 10–14 d after isolation. Dynabeads were magnetically removed before use in in vitro assays or adoptive transfer experiments.

Flow cytometry

Splenocytes and transduced T cells were stained with the indicated concentration I-A^K(VALVTDNAVYQWSME)-PE tetramer for 1 h at 37 degrees. Before surface staining, Fc receptors were blocked with anti-CD16/32 TruStain FcX (BioLegend) for 15 min on ice. Cells were then washed and stained for surface antigens on ice for 15–30 min. Dead cells were excluded with either 4,6-diamidino-2-phenylindole (DAPI), LIVE/DEAD Fixable Yellow (Thermo Fisher) or Fixable Viability Dye eFluor 780 (Thermo Fisher). Fluorescently conjugated antibodies specific for the following murine antigens were used in this study: CD45 (30-F11, 103131, BioLegend), CD4 (RM4-5, 100509, BioLegend), Thy1-1 (OX-7, 202523, BioLegend), TRBV8.3 (1B3.3, 553663, BD Biosciences), PD-1 (29F.1A12, 135219, BioLegend), CD69 (H1.2F3, 104513, BioLegend), TRBV14 (J9.19, 553258, BD Biosciences), TRBV4 (KT4, 553365, BD Biosciences), TCRb (H57-597, 20-5961, Tonbo), pERK1/2 (4B11B69, 675507, BioLegend), I-A/I-E (M5/114.15.2, 17-5321-82, eBiosciences), B220 (RA3-6B2, 25-0452-82, Invitrogen), CD3 (17A2, 100217, BioLegend), CD62L (MEL-14, 20-0621-U025, Tonbo), CD44 (IM7, 561860, BD Biosciences), Ly-6A/E (F13-161.7, 108123, BioLegend), CD8 (53-6.7, 35-0081-U025, Tonbo) and CD40L (MR1, 106505, BioLegend). All surface-staining antibodies listed were used at a 1:200 dilution. Anti-pERK1/2 was used at a 1:50 dilution for intracellular staining. Data were collected on a BD FACS Celesta or BD LSR-II using BD FACSDiva software and analyzed using FlowJo.

In vitro T cell functional assays

For splenocyte co-culture assays, 2×10^4 transduced T cells were co-cultured with 2×10^5 splenocytes pulsed overnight with indicated concentrations of $CLTC_{H192>Q}$ (SLNTVALVTDNAVYQWSMEG) or wild-type CLTC (SLNTVALVTDNAVYHWSMEG) peptide in 96-well U-bottom plates. Supernatants were collected after 18–24 h and IFN-γ was measured by ELISA (BD Bioscience). For measuring levels of proximal TCR signaling, 5×10^4 transduced T cells were co-cultured with 1×10^5 splenocytes pulsed overnight with 1 µg ml^{-1} $CLTC_{H129>Q}$ peptide in 96-well U-bottom plates. Cells were centrifuged for 10 s at 400*g* to initiate contact between T cells and APCs. After incubation for 5 min at 37 °C, the reaction was stopped on ice for 30 s. The plate was then centrifuged at 311*g* for 2 min, supernatants were discarded and wells were vortexed to resuspend cells in remaining volume. Cells were immediately fixed with ice-cold 4% paraformaldehyde for 15 min on ice, followed by two washes with FACS buffer. Cells were then permeabilized with ice-cold 90% methanol for 15 min, followed by an additional two washes with FACS buffer. Cells were then stained intracellularly for phosphorylated ERK1/2 for 30 min at room temperature, before washing twice with FACS buffer and analyzing levels of phosphorylated ERK1/2 by flow cytometry.

Adoptive transfers and in vivo treatments

Naive or tumor-bearing C3H/HeJ mice were injected i.v. via the tail vein with the indicated number of $CD4^+$ T cells in 200 µl 1× HBSS at the

indicated time points. Where indicated, $CD4^+$ T cells were first labeled with CTV (Thermo Fisher) according to manufacturer's instructions. Depletion of $CD8^+$ T cells was achieved by intraperitoneal (i.p.) injection of 200 µg anti-CD8 (116-13.1, BE0118, BioXCELL) or IgG2a (C1.18.4, BE0085, BioXCELL) isotype control at D4 and D0 relative to tumor cell injection for primary tumor immunity experiments. To deplete $CD8^+$ T cells during therapeutic experiments, 200 µg anti-CD8 was injected i.p. immediately following adoptive transfer of $CD4^+$ T cells and every 7 d for the duration of the experiment. CD40L was blocked in vivo by i.p. administration of 200 µg anti-CD40L (MR1, BE0017-1, BioXCELL) compared to Armenian hamster IgG (PIP, BE0260, BioXCELL) isotype control on D0 and D2 for primary tumor immunity experiments. Where indicated, tumor-bearing mice were treated with 150 mg kg^{-1} cyclophosphamide monohydrate (Sigma) dissolved in 1× PBS i.p. 1 d before T cell transfer. Tumor volume was calculated by the equation $V = (l \times w^2) / 2$ where l and w correspond to the longer and shorter perpendicular diameters respectively. For therapeutic experiments, mice were treated once tumor volumes reached 100–250 mm^3. Mice were randomized before initiating treatment.

RNA sequencing and bioinformatic analyses

RNA paired-end sequencing reads were obtained using Illumina's NovaSeq 6000 system. FastQC (v.0.11.9) and Trimmomatic (v.0.32) were used to run quality control and trim low-quality control reads. The paired ends that passed Illumina filters were filtered for reads aligning to tRNA, rRNA, adaptor sequences and spike-in controls. The reads were then aligned to the GRCm38 reference genome and Gencode v.M9 annotations using STAR (v.2.6.1c)[56]. DUST scores were calculated with PRINSEQ Lite (v.0.20.3)[57] and low-complexity reads (DUST > 4) were removed from the BAM files. The alignment results were parsed via SAMtools[58] to generate SAM files. Read counts to each genomic feature were obtained with the featureCounts program (v.1.6.5)[59]. After removing absent features (zero counts in all samples), the raw counts were then imported to R/Bioconductor package DESeq2 (ref. 60) to identify differentially expressed genes among samples. *P* values for differential expression were calculated using the Wald test for differences between the base means of two conditions. These *P* values were then adjusted for multiple test correction using the Benjamini–Hochberg algorithm[61] to control the false discovery rate. We considered genes differentially expressed between two groups of samples when the DESeq2 analysis resulted in an adjusted *P* value of <0.05 and the absolute value of the log fold change in gene expression was >1. Variance stabilizing transformation (DESeq2 v.1.24.0) was applied to the read counts for all samples. As there were samples from multiple mapping runs, adjustment of batch effect with outcome of interest as disease state was performed using ComBat (sva v.3.32.1).

Statistics

Statistical analyses were performed with Prism 9 (GraphPad Software). Statistical tests and significance are indicated in the figure legends.

Study approval

All animal studies were approved by The La Jolla Institute for Immunology Institutional Animal Care and Use Committee Animal Protocol AP00001026.

Reporting summary

Further information on research design is available in the Nature Portfolio Reporting Summary linked to this article.

Data availability

Bulk RNA-seq data have been uploaded to the NCBI Gene Expression Omnibus and are accessible under accession no. GSE229221. The mouse reference genome GRCm38 is accessible through GenBank under accession no. GCA_000001635.2. Source data are provided with this paper.

References

55. Lefranc, M. P. IMGT, the international imMunoGeneTics information system. *Cold Spring Harb. Protoc.* **6**, 595–603 (2011).
56. Dobin, A. et al. STAR: ultrafast universal RNA-seq aligner. *Bioinformatics* **29**, 15–21 (2013).
57. Schmieder, R. & Edwards, R. Quality control and preprocessing of metagenomic datasets. *Bioinformatics* **27**, 863–864 (2011).
58. Li, H. et al. The Sequence Alignment/Map format and SAMtools. *Bioinformatics* **25**, 2078–2079 (2009).
59. Liao, Y., Smyth, G. K. & Shi, W. featureCounts: an efficient general purpose program for assigning sequence reads to genomic features. *Bioinformatics* **30**, 923–930 (2014).
60. Love, M. I., Huber, W. & Anders, S. Moderated estimation of fold change and dispersion for RNA-seq data with DESeq2. *Genome Biol.* **15**, 550 (2014).
61. Benjamini, Y. & Hochberg, Y. Controlling the false discovery rate: a practical and powerful approach to multiple testing. *J. R. Stat. Soc. Ser. B Methodol.* **57**, 289–300 (1995).

Acknowledgements

We acknowledge D. Hinz, C. Dillingham and C. Kim at The La Jolla Institute for Immunology Flow Cytometry Core for technical assistance with FACS-sorting experiments. We also acknowledge S. Alarcón and H. Dose from The La Jolla Institute for Immunology Next Generation Sequencing Core for technical assistance in sample preparation and RNA sequencing. The MSGV1 vector was a gift from C. Hinrichs (Addgene plasmid #122728). I-A^K (VALVTDNAVYQWSME) tetramers conjugated to PE and APC were provided by the National Institutes of Health Tetramer Core Facility. Figure schematics created with BioRender. This work was made possible by funds from the National Institutes of Health (UO1 DE028227) and the San Diego Center for Precision Immunotherapy to S.P.S., and the Sandor and Rebecca Shapery family to S.E.B.

Author contributions

S.E.B. and S.P.S. designed the experiments. S.E.B., A.B., R.R.T., M.S.N., R.Q.G., K.S.Z. and J.S.D. performed experiments. L.C. and A.L.R.P. analyzed transcriptome data with guidance from B.P. S.E.B. analyzed data and performed statistical analyses. S.P.S., E.E.W.C. and A.M.M. secured funding for the study. S.E.B. prepared the figures and wrote the manuscript with S.P.S.

Competing interests

M.S.N., A.M.M., B.P. and S.P.S. are listed as inventors on patents related to tumor-specific TCRs. S.P.S. serves on the scientific advisory boards of Telesis Bio, 3T Biosciences and Grit Bio. All other authors declare no competing interests.

Additional information

Extended data is available for this paper at https://doi.org/10.1038/s41590-023-01543-9.

Supplementary information The online version contains supplementary material available at https://doi.org/10.1038/s41590-023-01543-9.

Correspondence and requests for materials should be addressed to Stephen P. Schoenberger.

Peer review information *Nature Immunology* thanks William Haining and the other, anonymous, reviewer(s) for their contribution to the peer review of this work. Primary Handling Editor: J. Wilson, in collaboration with the *Nature Immunology* team.

https://doi.org/10.1038/s41590-023-01543-9

a

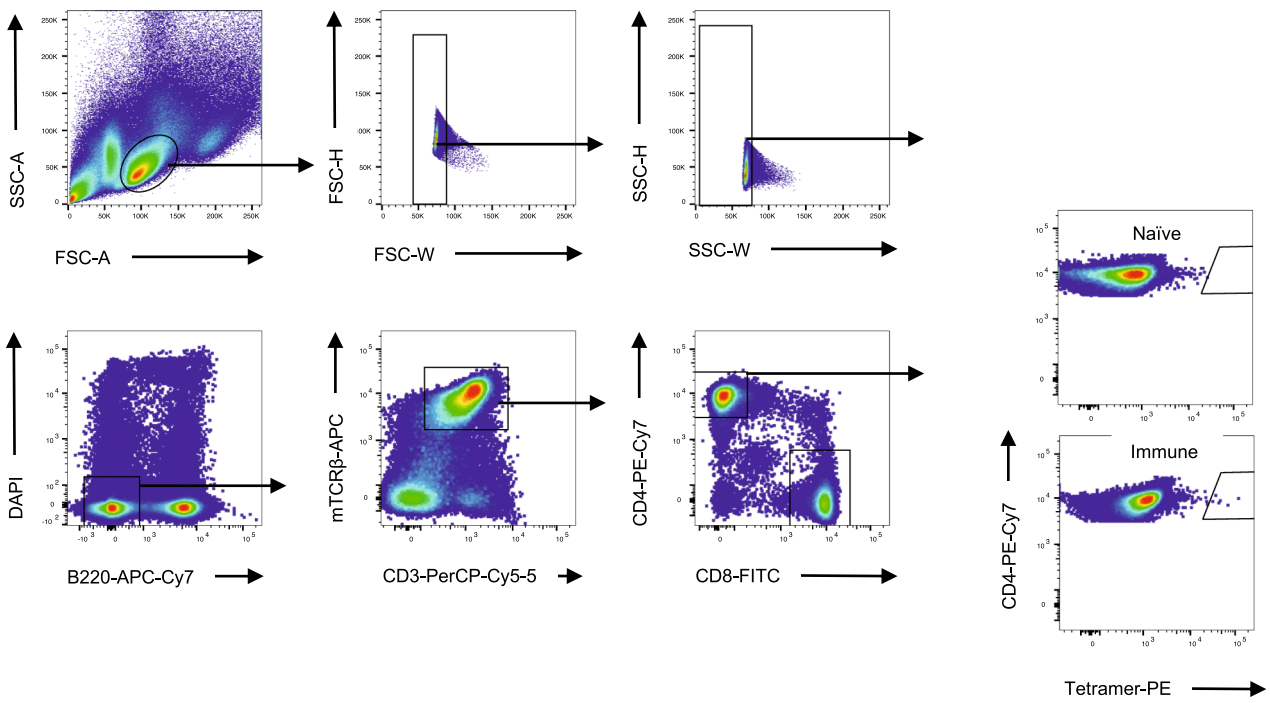

b

TCR ID	TRAV/TRAJ	CDR3 α	TRBV/TRBJ	CDR3 β	MFI Tetramer (Average)
1	TRAV9D-4*01 TRAJ5*01	CALS**P**GTQVVGQLTF	TRBV13-1*01 TRBJ1-1*01	CASSGGPNTEVFF	1779
2	TRAV9D-4*01 TRAJ5*01	CALS**A**GTQVVGQLTF	TRBV13-1*01 TRBJ1-1*01	CASSGGPNTEVFF	2637
3	TRAV7-5*01 TRAJ26*01	CAMSPRTQGLTF	TRBV31*02 TRBJ2-7*01	CAWLSLPGQYEQYF	78
4	TRAV7D-3*01 TRAJ21*01	CAVNYNVLYF	TRBV2*01 TRBJ203*01	CASSRDNSAETLYF	147

Extended Data Fig. 1 | Gating strategy for sorting CLTC$_{H1129Q}$-specific CD4$^+$ T cells and TCR characteristics. a Representative gating strategy for sorting CLTC$_{H1129>Q}$-specific CD4$^+$ T cells. **b** Table of TCR genes and tetramer median fluorescence intensity for expanded T cell clones.

https://doi.org/10.1038/s41590-023-01543-9

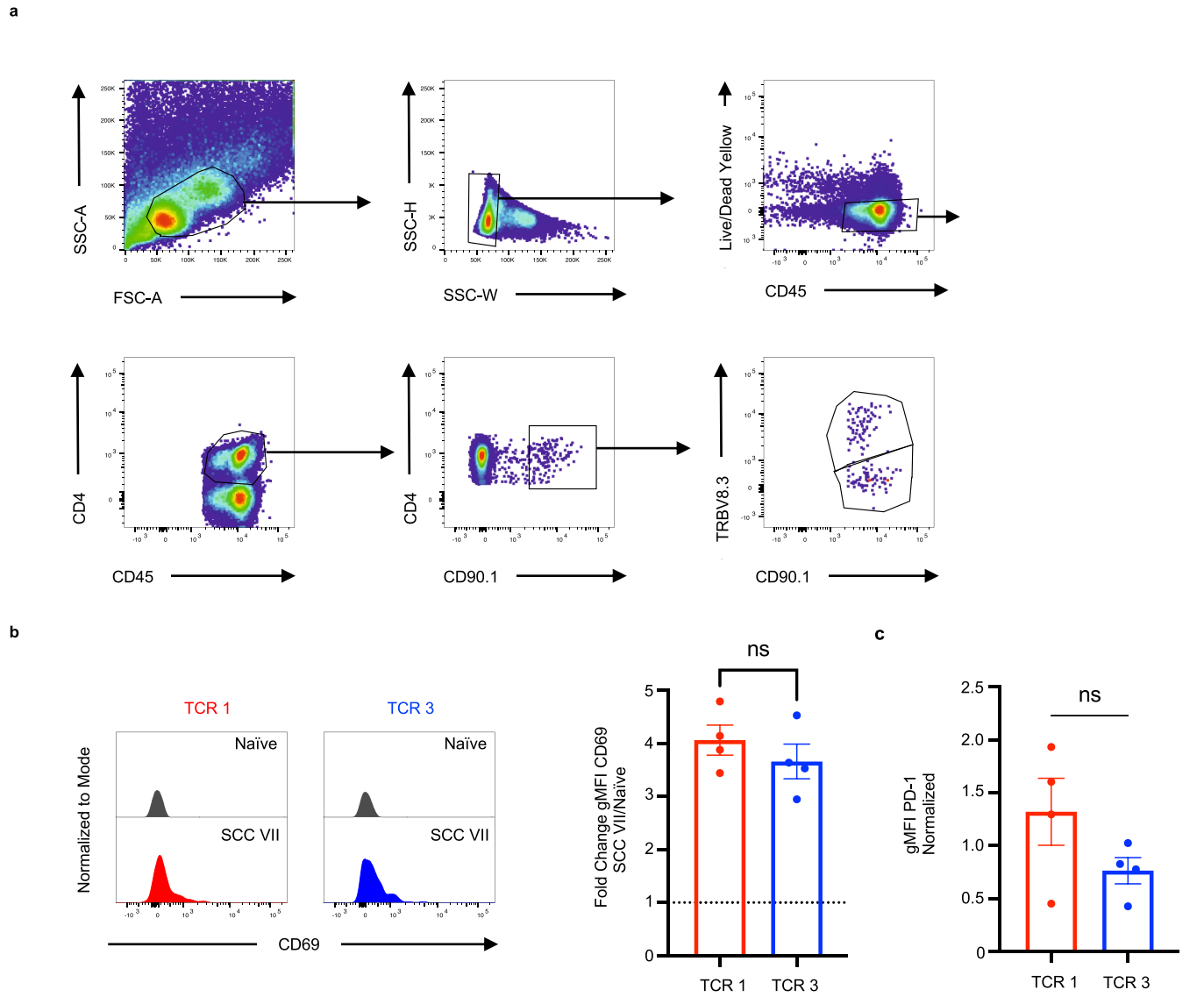

Extended Data Fig. 2 | CLTC$_{HI29Q}$-specific CD4$^+$ T cell activation in the tdLN and tumor during tumorigenesis. a Representative gating strategy to identify adoptively transferred cells expressing TCR 1 and TCR 3. **b** Representative histograms (left) and quantification (right) of CD69 upregulation by cells expressing TCR 1 and TCR 3 in the tdLN in SCC VII tumor-bearing mice compared to mice without tumors. Mean +/− SEM, $n = 4$ mice per group, representative of two independent experiments. ns $p > 0.05$ two-tailed unpaired T-test. **c** Quantification of PD-1 gMFI normalized to FMO for TCR 1 and TCR 3 in the tumor. Mean +/− SEM, $n = 4$ mice per group, representative of two independent experiments. ns $p > 0.05$ two-tailed unpaired T-test.

https://doi.org/10.1038/s41590-023-01543-9

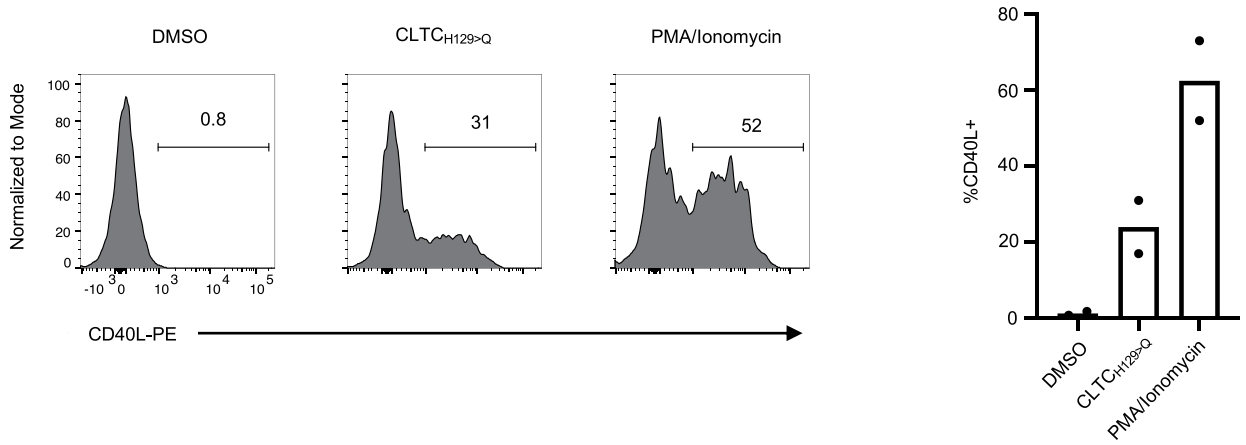

Extended Data Fig. 3 | CD4$^+$ T cells expressing TCR 1 upregulate CD40L upon antigen recognition. Flow cytometry histograms (left) and quantification (right) of CD40L expression by CD4$^+$ T cells expressing TCR 1 stimulated with unpulsed splenocytes, splenocytes pulsed with 1 µg/mL CLTC$_{H129>Q}$ peptide, or PMA/Ionomycin. Mean +/− SEM, Data represents two independent experiments.

https://doi.org/10.1038/s41590-023-01543-9

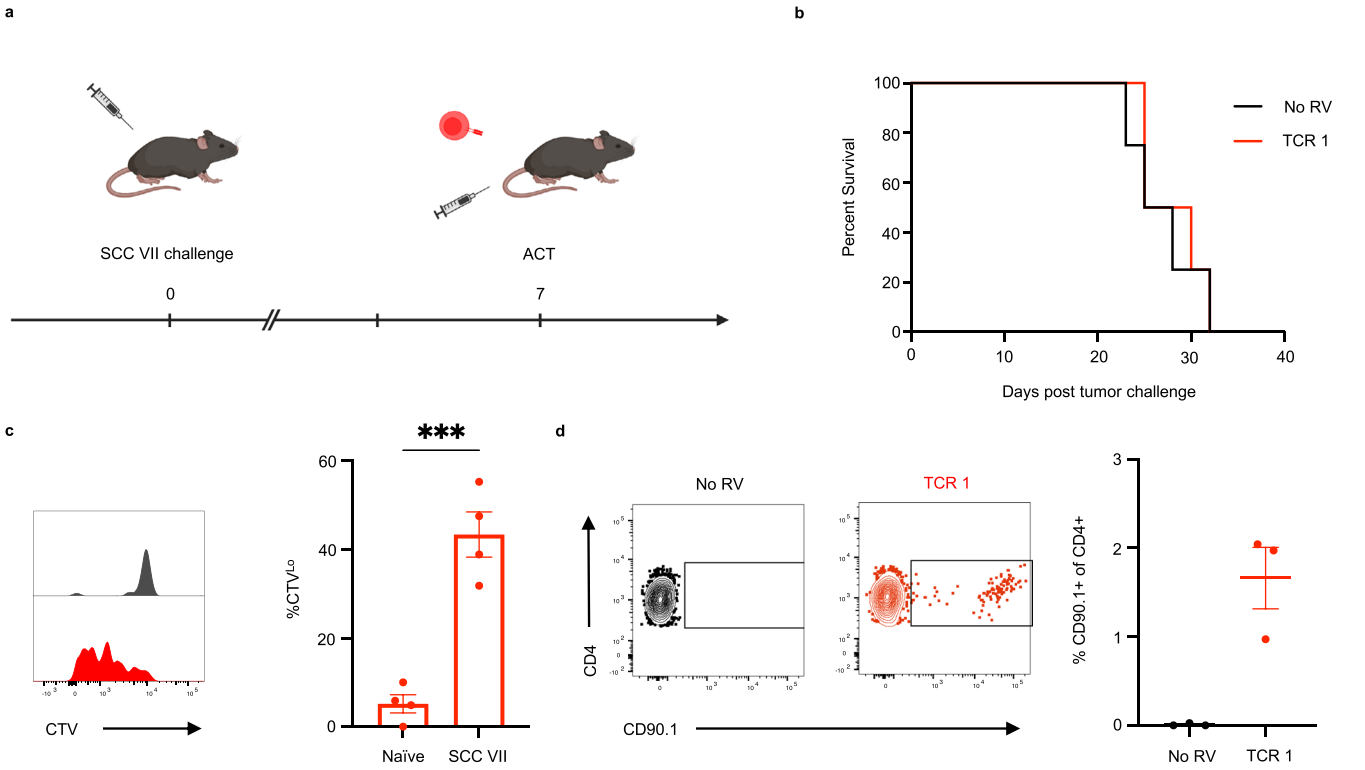

Extended Data Fig. 4 | Adoptive transfer of CLTC$_{H129Q}$-specific CD4$^+$ T cells without cyclophosphamide does not improve survival. a Experimental scheme of therapeutic adoptive transfer experiments. **b** Survival curves comparing mice receiving 3×10^6 CLTC^{H129Q}-specific cells expressing TCR 1 or an equal number of mock transduced polyclonal activated CD4$^+$ T cells. $n = 4$ mice per group, representative of three independent experiments. **c** Representative flow cytometry histograms (left) and quantification (right) of CellTrace violet dilution in the tdLN following adoptive transfer of CLTC^{H129Q}-specific CD4$^+$ T cells to either naïve mice or mice with established SCC VII tumors. Mean +/− SEM, $n = 4$ mice per group, *** p <=0.0003 two-tailed unpaired T-test. **d** Representative flow cytometry plots (left) and quantification (right) of the frequency of adoptively transferred CD90.1$^+$ CD4$^+$ T cells present in tumors from treated mice. Mean +/− SEM, $n = 3$ mice per group, representative of three independent experiments.

https://doi.org/10.1038/s41590-023-01543-9

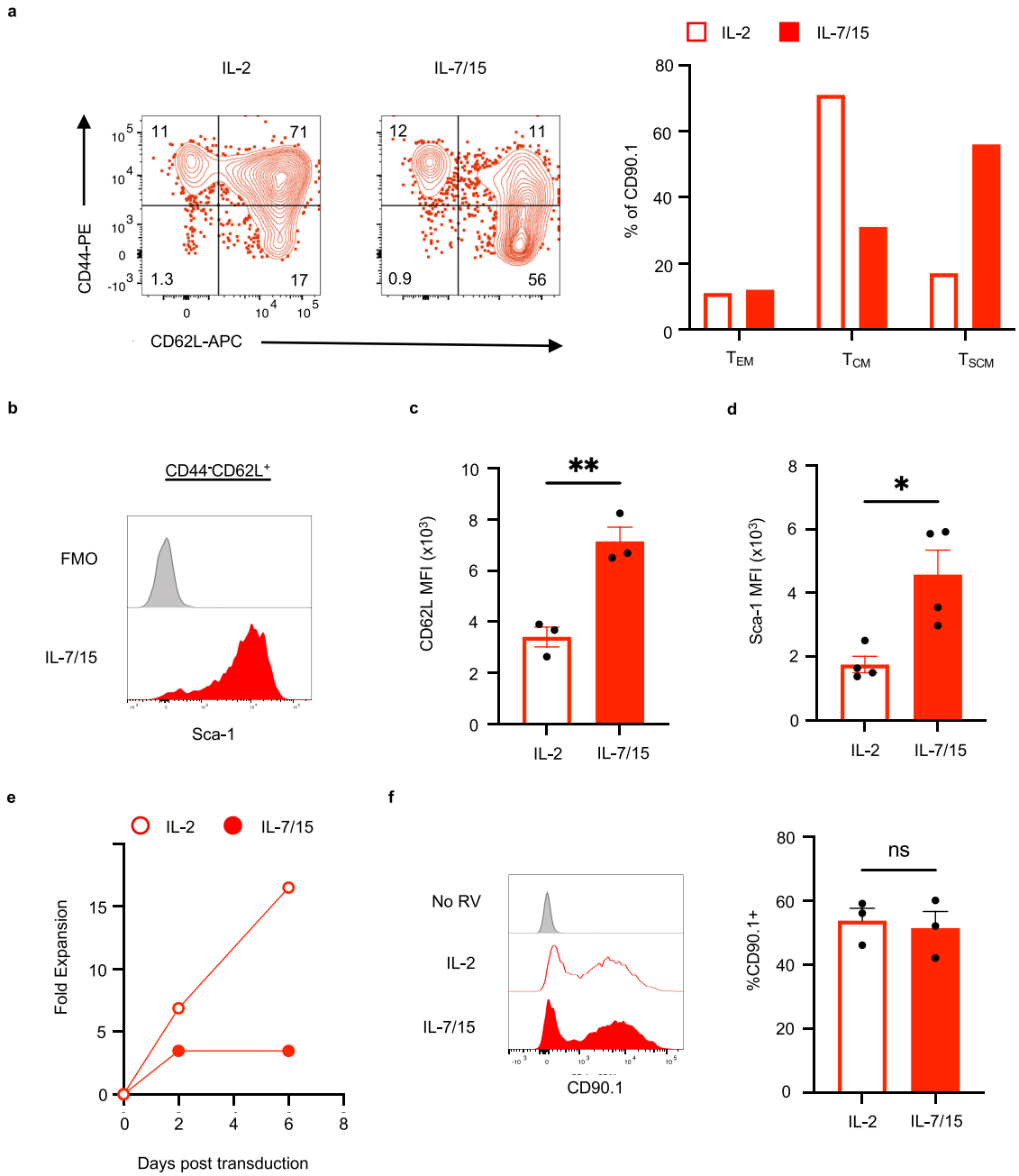

Extended Data Fig. 5 | *In vitro* phenotype of TCR-engineered cells cultured in either IL-2 or IL-7 and IL-15. a Flow cytometry plots (left) and quantification (right) of CD44 and CD62L expression by $CD4^+$ T cells cultured with indicated cytokines. T_{EM}, T_{CM} and T_{SCM} are designated as CD44 + CD62L−, CD44 + CD62L + and CD44loCD62L+ respectively. Representative of four independent experiments. **b** Flow cytometry histograms of Sca-1 expression by IL-7/15-treated cells. Representative of four independent experiments. **c** Quantification of CD62L expression represented as the median fluorescence intensity for cells cultured in either IL-2 or IL-7/15. Mean +/− SEM, data represents three independent experiments. ** p = 0.0053 two-tailed unpaired T-test. **d** Quantification of Sca-1 expression represented as the median fluorescence intensity for cells cultured in either IL-2 or IL-7/15. Mean +/− SEM, data represents four independent experiments. * p = 0.0131 two-tailed unpaired T-test. **e** Fold expansion *in vitro* plotted over time for TCR-engineered cells cultured in IL-2 or IL-7/15. Data representative of four independent experiments. **f** Flow cytometry histograms (left) and quantification (right) of CD90.1 expression by transduced T cells cultured in indicated cytokines. Mean +/− SEM, data represents three independent experiments, ns p > 0.05 two-tailed unpaired T-test.

nature portfolio

Corresponding author(s): Stephen P. Schoenberger

Last updated by author(s): 5/16/2023

Reporting Summary

Nature Portfolio wishes to improve the reproducibility of the work that we publish. This form provides structure for consistency and transparency in reporting. For further information on Nature Portfolio policies, see our Editorial Policies and the Editorial Policy Checklist.

Statistics

For all statistical analyses, confirm that the following items are present in the figure legend, table legend, main text, or Methods section.

n/a	Confirmed	
☐	☒	The exact sample size (*n*) for each experimental group/condition, given as a discrete number and unit of measurement
☐	☒	A statement on whether measurements were taken from distinct samples or whether the same sample was measured repeatedly
☐	☒	The statistical test(s) used AND whether they are one- or two-sided *Only common tests should be described solely by name; describe more complex techniques in the Methods section.*
☐	☒	A description of all covariates tested
☐	☒	A description of any assumptions or corrections, such as tests of normality and adjustment for multiple comparisons
☐	☒	A full description of the statistical parameters including central tendency (e.g. means) or other basic estimates (e.g. regression coefficient) AND variation (e.g. standard deviation) or associated estimates of uncertainty (e.g. confidence intervals)
☐	☒	For null hypothesis testing, the test statistic (e.g. *F*, *t*, *r*) with confidence intervals, effect sizes, degrees of freedom and *P* value noted *Give P values as exact values whenever suitable.*
☒	☐	For Bayesian analysis, information on the choice of priors and Markov chain Monte Carlo settings
☒	☐	For hierarchical and complex designs, identification of the appropriate level for tests and full reporting of outcomes
☐	☒	Estimates of effect sizes (e.g. Cohen's *d*, Pearson's *r*), indicating how they were calculated

Our web collection on statistics for biologists contains articles on many of the points above.

Software and code

Policy information about availability of computer code

Data collection	BD FACSDiva was used to collect flow cytometry data
Data analysis	Flow cytometry data were analyzed using FlowJo v10.8.2. Data analysis, visualization, and statistical analyses were performed with Prism 9. For RNA-seq data, the following analysis packages were used: FastQC (v0.11.9), Trimmomatic (v.0.32), STAR (v2.6.1c) , PRINSEQ Lite (v 0.20.3), SAMtools (v1.17), featureCounts (v1.6.5), DESeq2 (1.24.0), ComBat (3.32.1)

For manuscripts utilizing custom algorithms or software that are central to the research but not yet described in published literature, software must be made available to editors and reviewers. We strongly encourage code deposition in a community repository (e.g. GitHub). See the Nature Portfolio guidelines for submitting code & software for further information.

Data

Policy information about availability of data

All manuscripts must include a data availability statement. This statement should provide the following information, where applicable:

- Accession codes, unique identifiers, or web links for publicly available datasets
- A description of any restrictions on data availability
- For clinical datasets or third party data, please ensure that the statement adheres to our policy

Data Availability Statement: Bulk RNA-seq data has been uploaded to NCBI GEO and is accessible under accession number GSE229221. Source data are provided with this article.

Human research participants

Policy information about studies involving human research participants and Sex and Gender in Research.

Reporting on sex and gender	N/A
Population characteristics	N/A
Recruitment	N/A
Ethics oversight	N/A

Note that full information on the approval of the study protocol must also be provided in the manuscript.

Field-specific reporting

Please select the one below that is the best fit for your research. If you are not sure, read the appropriate sections before making your selection.

☒ Life sciences ☐ Behavioural & social sciences ☐ Ecological, evolutionary & environmental sciences

For a reference copy of the document with all sections, see nature.com/documents/nr-reporting-summary-flat.pdf

Life sciences study design

All studies must disclose on these points even when the disclosure is negative.

Sample size	Sample sizes for animal experiments were chosen in line with published results for similar experiments.
Data exclusions	No data were excluded from this study.
Replication	All experiments were replicated at least once with number of replicate experiments indicated in the figure legends.
Randomization	For therapeutic animal experiments, mice were randomized prior to treatment initiation to account for variation in tumor size. For prophylactic experiments where treatments were administered prior to tumor initiation, animals of the same age were used and separate cages received separate treatments.
Blinding	Blinding was not possible for in vivo tumor studies as tumor measurements were only taken by one researcher. For all other experiments blinding was not necessary.

Reporting for specific materials, systems and methods

We require information from authors about some types of materials, experimental systems and methods used in many studies. Here, indicate whether each material, system or method listed is relevant to your study. If you are not sure if a list item applies to your research, read the appropriate section before selecting a response.

Materials & experimental systems

n/a	Involved in the study
☐	☒ Antibodies
☐	☒ Eukaryotic cell lines
☒	☐ Palaeontology and archaeology
☐	☒ Animals and other organisms
☒	☐ Clinical data
☒	☐ Dual use research of concern

Methods

n/a	Involved in the study
☒	☐ ChIP-seq
☐	☒ Flow cytometry
☒	☐ MRI-based neuroimaging

Antibodies

Antibodies used	Fluorescently conjugated antibodies specific for the following murine antigens were used in this study: CD45 (30-F11, 103131, Biolegend), CD4 (RM4-5, 100509, Biolegend), Thy1-1 (OX-7, 202523, Biolegend), TRBV8.3 (1B3.3, 553663, BD Biosciences), PD-1 (29F.1A12, 135219, Biolegend), CD69 (H1.2F3, 104513, Biolegend), TRBV14 (J9.19, 553258, BD Biosciences), TRBV4 (KT4, 553365, BD Biosciences), TCRb (H57-597, 20-5961, Tonbo), pERK1/2 (4B11B69, 675507, Biolegend), I-A/I-E (M5/114.15.2, 17-5321-82, eBiosciences), B220 (RA3-6B2, 25-0452-82, Invitrogen), CD3 (17A2, 100217, Biolegend), CD62L (MEL-14, 20-0621-U025, Tonbo),

	CD44 (IM7, 561860, BD Biosciences), Ly-6A/E (F13-161.7, 108123, Biolegend), CD8 (53-6.7, 35-0081-U025, Tonbo), CD40L (MR1, 106505, Biolegend). All surface staining antibodies listed were used at a 1:200 dilution. Anti-pERK1/2 antibody was used at a 1:50 dilution for intracellular staining. The following antibodies were used for in vivo depletions/blockades: anti-CD8 (116-13.1, BE0118, BioXCELL), IgG2a (C1.18.4, BE0085, BioXCELL), anti-CD40L (MR1, BE0017-1, BioXCELL), Armenian hamster IgG (PIP, BE0260, BioXCELL)
Validation	All antibodies were validated for use in mice and for the indicated applications on the manufacturers websites (flow cytometry, in vivo depletion for 116-13.1, in vivo blocking for MR1.)

Eukaryotic cell lines

Policy information about cell lines and Sex and Gender in Research

Cell line source(s)	SCC VII tumor cell lines were a gift from Michael Beckett (mbeckett@uchicago.edu) and originally derived from a spontaneous murine abdominal wall tumor in the lab of Dr. Herman Suit at Harvard University. 58a-b- were a gift from Bernard Malissen (bernardm@ciml.univ-mrs.fr
Authentication	Cell lines were not authenticated
Mycoplasma contamination	All cell lines tested negative for mycoplasma
Commonly misidentified lines (See ICLAC register)	No commonly misidentified cell lines were used.

Animals and other research organisms

Policy information about studies involving animals; ARRIVE guidelines recommended for reporting animal research, and Sex and Gender in Research

Laboratory animals	8-12 week old female C3H/Hej mice were used in these studies
Wild animals	This study did not involve wild animals
Reporting on sex	Female mice were used because the tumor cell line (SCC VII) was derived from a female mouse
Field-collected samples	This study did not involve field collected samples
Ethics oversight	The animal study protocol was approved by the La Jolla Institute for Immunology Institutional Animal Care and Use Committee (IACUC)

Note that full information on the approval of the study protocol must also be provided in the manuscript.

Flow Cytometry

Plots

Confirm that:

☒ The axis labels state the marker and fluorochrome used (e.g. CD4-FITC).

☒ The axis scales are clearly visible. Include numbers along axes only for bottom left plot of group (a 'group' is an analysis of identical markers).

☒ All plots are contour plots with outliers or pseudocolor plots.

☒ A numerical value for number of cells or percentage (with statistics) is provided.

Methodology

Sample preparation	Samples were prepared as described in the materials and methods. Mouse spleens, tumors, and inguinal lymph nodes were surgically removed. Spleens were dissociated manually and cell suspensions were passed through a 70 uM strainer. Prior to use as antigen presenting cells in T cell in vitro assays, red blood cells were lysed with ACK lysis buffer. Lymph nodes and subcutaneous tumors were minced into small (<2mm) pieces with dissection scissors. Tissue fragments were enzymatically dissociated in 20 ug/mL Liberase (Roche) and 20 ug/mL DNase I (Roche) at 37 degrees C for 30 minutes. Single cells were then passed through a 70 uM strainer.
Instrument	BD LSR-II and BD FACS Celesta were used for data aquisition
Software	Flow cytometry data was collected using BD FACSDiva software and anlyzed with FlowJo v10.8.2
Cell population abundance	For tetramer sorting experiments, given the low total number of cells, no post-sort purity assessment was made and all single cells were used for TCR sequencing experiments.

Gating strategy

Where relevant, gating strategies have been included as supplemental figures. Tetramer binding CD4+ T cells from mice were pregated as live, B220-, CD3+, mTCRb+, CD8-, CD4+ cells. In adoptive transfer experiments, transferred TCR-engineered CD4 + T cells were identified as live, CD45+, CD4+, CD90.1+ cells.

☒ Tick this box to confirm that a figure exemplifying the gating strategy is provided in the Supplementary Information.